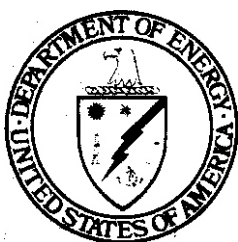


KES

DOE/ER-OO46/22



Damage Analysis and Fundamental Studies

Quarterly Progress Report
April-June 1985

August 1985

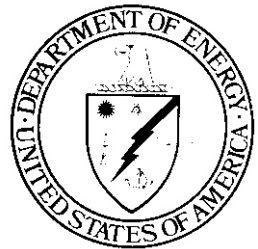
U.S. Department of Energy
Office of Energy Research
Office of Fusion Energy
Washington, DC 20545
B&R No. AT-15-O2-O3-O4

NOTICE

This report was prepared as an account of work sponsored by an agency of the United States Government. Neither the United States Government nor any agency thereof, nor any of their employees, nor any of their contractors, subcontractors or their employees, makes any warranty, express or implied, or assumes any legal liability or responsibility for the accuracy, completeness, or any third party's use or the results of such use of any information, apparatus, product, or process disclosed, or represents that its use would not infringe privately owned rights. Reference herein to any specific commercial product, process, or service by trade name, trademark, manufacturer, or otherwise, does not necessarily constitute or imply its endorsement, recommendation, or favoring by the United States Government or any agency thereof or its contractors or subcontractors.

Printed in the United States of America
Available from
National Technical Information Service
U.S. Department of Commerce
5285 Port Royal Road
Springfield, VA 22161

NTIS price codes
Printed copy: A 04
Microfiche copy: A01



Damage Analysis and Fundamental Studies

Quarterly Progress Report
April-June 1985

August 1985

U.S. Department of Energy
Office of Energy Research
Office of Fusion Energy
Washington, DC 20545
B&R No. AT-15-02-03-04

FOREWORD

This report is the thirtieth in a series of Quarterly Technical Progress Reports on *Damage Analysis and Fundamental Studies* (DAFS), which is one element of the Fusion Reactor Materials Program, conducted in support of the Magnetic Fusion Energy Program of the U.S. Department of Energy (DOE). The first eight reports in this series were numbered DOE/ET-0065/1 through 8. Other elements of the Fusion Materials Program are:

- Alloy Development for Irradiation Performance (ADIP)
- Plasma-Materials Interaction (PMI)
- Special Purpose Materials (SPM).

The DAFS program element is a national effort composed of contributions from a number of National Laboratories and other government laboratories, universities, and industrial laboratories. It was organized by the Materials and Radiation Effects Branch, DOE/Office of Fusion Energy, and a Task Group on *Damage Analysis and Fundamental Studies*, which operates under the auspices of that branch. The purpose of this series of reports is to provide a working technical record of that effort for the use of the program participants, the fusion energy program in general, and the DOE.

This report is organized along topical lines in parallel to a Program Plan of the same title so that activities and accomplishments may be followed readily, relative to that Program Plan. Thus, the work of a given laboratory may appear throughout the report. A chapter has been added on Reduced Activation Materials to accommodate work on a topic not included in the early program plan. The Contents is annotated for the convenience of the reader.

This report has been compiled and edited by N. E. Kenny under the guidance of the Chairman of the Task Group on *Damage Analysis and Fundamental Studies*, D. G. Doran, Hanford Engineering Development Laboratory (HEOL). Their efforts, those of the supporting staff of HEOL, and the many persons who made technical contributions are gratefully acknowledged. T. C. Reuther, Fusion Technologies Branch, is the DOE counterpart to the Task Group Chairman and has responsibility for the DAFS program within DOE.

G. M. Haas, Chief
Fusion Technologies Branch
Office of Fusion Energy

CONTENTS

	<u>Page</u>
Foreword	iii
CHAPTER 1: IRRADIATION TEST FACILITIES	1
1. <u>RTNS-II IRRADIATIONS AND OPERATIONS (LLNL)</u>	2
Irradiations were performed on 18 different experiments during this quarter. Several machine improvements were made. David Short was appointed Manager of the RTNS-II effective May 9, 1985, and Dale Heikkinen was appointed Deputy Manager.	
CHAPTER 2: DOSIMETRY AND DAMAGE PARAMETERS	4
1. <u>FISSION REACTOR DOSIMETRY - HFIR-RB2 (ANL)</u>	5
Dosimetry measurements and damage calculations were completed for the RB2 experiment in the removable beryllium position in HFIR. The maximum neutron fluence was $6.50 \times 10^{22} n/cm^2$ ($1.05 \times 10^{22} n/cm^2$ above 0.1 MeV) resulting in 11 dpa and 1450 appm helium in 316 stainless steel.	
2. <u>HELIUM PRODUCTION IN COPPER BY A THERMAL THREE-STAGE REACTION (RI, ANL)</u>	8
Cross sections have been deduced for four reactions that allow one to calculate total helium production in copper for high-fluence irradiations in HFIR.	
3. <u>ON ISOTOPIC ALLOYING TO TAILOR HELIUM PRODUCTION RATES IN MIXED SPECTRUM REACTORS (ORNL)</u>	13
Isotopic alloying is examined as a means of manipulating the ratio of helium transmutations to atom displacements in mixed spectrum reactors. It is based on artificially altering the relative abundances of the stable isotopes of nickel to systematically vary the fraction of ^{58}Ni in nickel-bearing alloys.	
CHAPTER 3: REDUCED ACTIVATION MATERIALS	24
1. <u>ACTIVATION CALCULATIONS WITH AN EXPANDED CROSS-SECTION LIBRARY (HEOL)</u>	25
The activation of a number of elements has been calculated for 10 and 40 MW-y/m ² exposures at a STARFIRE first wall location using a greatly expanded cross-section library and multiple time steps. The activation of critical radioisotopes increases nearly linearly with fluence.	
CHAPTER 4: RADIATION EFFECTS MECHANISMS AND CORRELATIONS	29
1. <u>THE MICROSTRUCTURAL EVOLUTION OF HEAVY-ION-IRRADIATED HT-9 FERRITIC STEEL EXAMINED IN CROSS SECTION (U. Wisconsin-Madison)</u>	30
HT-9 specimens were irradiated with 14-MeV Ni^{+3} ions to 200 dpa in the temperature range 300°C to 600°C and examined using a newly developed cross-section technique. Major features were dense dislocation loops at 300-400°C, chi-phase precipitates at 500°C, and the absence of significant damage at 600°C.	
2. <u>EFFECTS OF CAVITATION ON DAMAGE CALCULATIONS IN ION-IRRADIATED P7 ALLOYS (U. of Wisconsin-Madison)</u>	39
The depth-dependent void parameters extracted in cross section were used to model the effect of voids on the depth-dependent damage produced during 14-MeV nickel ion irradiation of alloy P7 (essentially high purity 316 stainless steel). Corrections applied to the dose at the peak swelling depth yield swelling rates approaching 0.7%/dpa.	

CHAPTER 1

IRRADIATION TEST FACILITIES

RTNS-II IRRADIATIONS AND OPERATIONS

D. W. Short and D. W. Heikkinen (Lawrence Livermore National Laboratory)

1.0 Objective

The objectives of this work are operation of RTNS-II (a 14-MeV neutron source facility), machine development, and support of the experimental program that utilizes this facility. Experimenter services include dosimetry, handling, scheduling, coordination, and reporting. RTNS-II is supported jointly by the U.S. and Japan and is dedicated to materials research for the fusion power program. Its primary use is to aid in the development of models of high-energy neutron effects. Such models are needed in interpreting and projecting to the fusion environment, engineering data obtained in other spectra.

2.0 Summary

Irradiations were performed on 18 different experiments during this quarter. Target air controller was rebuilt and column entrance electrode was replaced on the left machine. The vacuum system modifications on the right and left machines have been completed. Ion source development continues. David Short was appointed Manager of the RTNS-II effective May 9, 1985 and Dale Heikkinen was appointed Deputy Manager.

3.0 Program

Title: RTNS-II Operations (WZJ-16)

Principal Investigator: D. W. Short

Affiliation: Lawrence Livermore National Laboratory

4.0 Relevant DAFs Program Plan Task/Subtask

TASK II.A.2,3,4.

TASK II.B.3,4

TASK II.C.1,2,6,11,18.

5.0 Irradiation - D. W. short. D. W. Heikkinen and M. W. Guinan

During this quarter, irradiations (both dedicated and add-on) were done for the following people.

<u>Experimenter</u>	<u>P or A*</u>	<u>Sample Irradiated</u>
D. Heikkinen (LLNL)	A	Nb - dosimetry calibration
P. Cannon (HEDL)	P	Thermocouples and ceramic-metal seals - Neutron damage
C. Snead (BNL) and M. Guinan (LLNL)	A	Nb ₃ Sn-Ti alloys (mono filaments) - critical field, current and temperature
R. Flukiger (Karlsruhe) and M. Guinan (LLNL)	A	Nb ₃ Sn various multifilamentary alloys - critical field, current and temperature
J. S. Huang & M. Guinan (LLNL)	A	Al, Cu, Fe, Ni-Si, NiAl and Ni ₃ Al - defect cluster formation and phase transformation

Experimenter	P or A*	Sample Irradiated
J. S. Huang & M. Guinan (LLNL)	A	BN - evaluate cmting for high temperature furnace
R. Borg	A	K ₃ Fe(CN) ₆ - K cross sections
K. Abe (Tohoku)	A	Sc and Mo - induced activity
H. Heinisch (HEDL) G. Pells (Harwell) F. Clinard (LANL) M. Kiritani (Hokkaido) R. Ohshima (Osaka) H. Yoshida (Kyoto) K. Abe (Tohoku) H. Matsui (Tohoku) H. Kayano (Tohoku) H. Kawanishi (Tokyo) N. Igata (Tokyo) Y. Shimomura (Hiroshima) N. Yoshida (Kyushu)	P	Metals - displacement damage & mechanical properties. Ceramics - neutron damage - irradiated at 90% and 290%
S. Iwasaki (Tohoku)	A	²⁷ Al(n,2n) - cross section
S. Iwasaki (Tohoku)	A	Pb(n,2n) - cross section
S. Iwasaki (Tohoku)	A	SS & Ni alloy - tensile
D. Tucker (LANL)	P	Polymer - mechanical
E. Franco (ARACOR)	A	Layered synthetic microstructures - Neutron damage
E. Dalder (LLNL)	A	Copper alloys - post irradiation activation analysis
J. McDonald (HEDL)	P	Cargon - Neutron kerm
J. Huang, M. Guinan & P. Hahn (LLNL)	P	Cu ₃ Au at 4.2% - in-situ measurements of resistivity during irradiation & subsequent annealing.
J. Huang, M. Guinan & P. Hahn (LLNL)	P	Cu ₃ Au at 300-450°K - in-situ measurements of resistivity during irradiation & subsequent annealing.

* P = primary, A = add-on

5.1 RTNS-II Status - D. W. Short and D. W. Heikkinen

Target air controller for the left machine was rebuilt.

Accelerator column entrance electrode was replaced on the left machine.

Ion source development continues on the right machine.

6.0 Future Work

Irradiations will be continued for D. Heikkinen (UW), H. Heinisch et al., S. Iwasaki (Tohoku). Also during this period, irradiations for A. Kohyama (Tokyo), T. Yoshiie (Hokkaido) and H. Kawanishi (Tokyo) will be initiated.

CHAPTER 2

DOSIMETRY AND DAMAGE PARAMETERS

FISSION REACTOR DOSIMETRY - HFIR-RB2

L. R. Greenwood (Argonne National Laboratory)

1.0 Objective

To characterize neutron irradiation experiments in terms of neutron fluence, spectra, and damage parameters (dpa, gas production, transmutation).

2.0 Summary

Dosimetry measurements and damage calculations have been completed for the RB2 experiment in the removable beryllium position in HFIR. The maximum neutron fluence was $6.50 \times 10^{22} \text{ n/cm}^2$ ($1.05 \times 10^{22} \text{ n/cm}^2$ above 0.1 MeV) resulting in 10.8 dpa and 1448 appm helium in 316 stainless steel.

The status of all other experiments is summarized in Table I.

Table I. Status of Dosimetry Experiments

ORR	- W E 1 - W E 2 - W E 4A1 - W E 4A2 - MFE 48 - TBC 07 - TRIO-Test - TRIO-1 - W Test - JP Test - J6, J7	completed 12/79 completed 06/81 Completed 12/81 completed 11/82 Completed 04/84 Completed 07/80 Completed 07/82 completed 12/83 Completed 03/84 Samples Received 03/85 Irradiations in progress	Omega west EBR II IPNS	- spectral Analysis - HEDL1 - HEDL2 - LANL 1 - X287 - spectral Analysis - LANLL (Hurley) - Hurley - Coltman	Completed 10/80 Completed 05/81 samples sent 04/85 Completed 08/84 cmpleted 09/81 Completed 01/82 Completed 06/82 Completed 02/83 Completed 08/83
HFIR	- CTR 32 - CTR 31, 34, 35 - T2, RB1 - T1, CTR 39 - CTR 40-45 - CTR 30, 36, 46 - RB2 - CTR 47-56 - JP 1-8 - Hf Test	completed 04/82 Completed 04/83 Completed 09/83 completed 01/84 completed 09/84 completed 03/85 completed 06/85 Irradiations in Progress Irradiations in Progress Planned for 08/85			

3.0 Program

Title: Dosimetry and Damage Analysis
Principal Investigator: L. R. Greenwood
Affiliation: Argonne National Laboratory

4.0 Relevant DAFS Program Plan Task/Subtask

Task II.A.1 Fission Reactor Dosimetry

5.0 Accomplishments and Status

Dosimetry measurements and damage calculations have been completed for the RB2 experiment in the removable beryllium position of the High Flux Isotopes Reactor (HFIR) at Oak Ridge National Laboratory. The experiment was irradiated for cycles 220-242 from February 7, 1982 until August 26, 1983 with a total exposure of 49253 MWd. The experiment contained Charpy and tensile specimens and is part of a series of three RB (removable beryllium) irradiations. Results from the RB1 experiment were reported previously.¹

Dosimeters were located at seven different positions in the RB2 assembly. Unfortunately, some of the monitors were damaged and others were lost during the disassembly. Full dosimetry sets were recovered from three positions and partial data from two other positions. Following gamma analysis, saturated activities were determined correcting for gamma absorption, the irradiation history, and burnup. The measured values are listed in Table II.

Table II. Measured Activities for HPIR RB2

values at 100 MW With Burnup Corrections
Accuracy $\pm 2\%$ Unless Noted

Height, cm ^a	<u>Activation Rate, at/at-s</u>				
	⁵⁹ Co(n, γ) ^a	⁵⁸ Fe(n, γ)	⁵⁴ Fe(n,p)	⁴⁶ Ti(n,p)	⁵⁵ Mn(n,2n)
	($\times 10^{-8}$)	($\times 10^{-9}$)	($\times 10^{-11}$)	($\times 10^{-12}$)	($\times 10^{-14}$)
21.8	1.60	0.48	0.62	0.92	2.19
13.1	-	-	-	1.42	-
2.7	3.19	1.00	1.33	1.89	-
-3.2	3.09	1.05	1.27	1.78	4.46
-7.8	2.99	-	-	-	-

^aCo(n, γ) values $\pm 5\%$ due to large burnup corrections.

^bFe(n, γ) values $\pm 3\%$.

The activity data in Table II is well-described by a quadratic equation for the vertical flux gradient, as follows:

$$f(z) = a(1 + bz + cz^2) \quad (1)$$

where a = midplane value, $b = -2.48 \times 10^{-3}$, $c = -9.76 \times 10^{-4}$, and z is the height in cm.

The midplane values were used to adjust the flux spectrum using the STAYSL computer code. The adjusted spectrum was then used to compute damage parameters with the SPECTER² computer code. The fluence and damage values are listed in Table III. Since there is no detectable spectral gradient, equation (1) also describes damage gradients. In this case, the a term in equation (1) is any one of the midplane values in Table III with the exceptions of nickel and copper. In the nickel case, the thermal helium production and extra damage requires a separate calculation. This effect is illustrated for 316 stainless steel in Table IV.

We have recently discovered a new thermal helium effect for copper.³ However, this effect is much smaller than in the nickel case since a three-stage reaction is required from ⁶³Cu to ⁶⁴Zn to ⁶⁵Zn which then produces helium from a thermal reaction. In the present case, this would add about 18.1 appm helium and 0.037 extra dpa at midplane.

6.0 References

1. L. R. Greenwood, Damage Analysis and Fundamental Studies Quarterly Progress Report, DOE/ER-0046/15, pp. 5-9, November 1983.
2. L. R. Greenwood and R. K. Smith, SPECTER: Neutron Damage Calculations for Materials Irradiations, ANL/FPP/TM-197, January 1985.
3. D. W. Kneff, L. R. Greenwood, B. M. Oliver, R. P. Skowronski, and E. L. Callis, "Helium Production in Copper by a Thermal Three-Stage Reaction," Proc. Int. Conf. on Nucl. Data for Basic and Applied Science, Santa Fe, NM., May 13-17, 1985 (to be published).

7.0 Future Work

Analysis is in progress for the J6 prototype in the ORR. Plans are being made to test the effect of a hafnium shield in the RB position in WIR. The dosimeters from the T3 experiment in HPIR were severely damaged and could not be analyzed. We are now exploring alternate methods to determine the exposure for this irradiation.

Table III. Neutron Fluence and Damage Parameters for RB2

values at midplane; use equation (1) for gradients

<u>Energy</u>	<u>Neutron Fluence, $\times 10^{22}$ n/cm²</u>
Total	6.50
Thermal (<.5 eV) ^a	4.15
Past (>.1 MeV)	1.05

<u>Element</u>	<u>DPA</u>	<u>He, appm</u>	
A1	14.66	6.93	
Ti	9.34	4.49	
V	10.34	0.24	
Cr	9.06	1.58	
Mn ^b	10.75	1.40	
Fe	7.90	2.80	
Co ^b	12.76	1.38	
Ni	Fast ⁵⁹ Ni Total	8.8 <u>19.5</u> 28.4	36. <u>11.089.</u> 11,125.
Cu ^c	Fast ⁶⁵ Zn Total	7.79 <u>.04</u> 7.83	2.51 <u>18.10</u> 20.61
Nb	7.44	0.51	
Mo	5.55		
316 SS ^d	10.76	1448.	

^aMultiply $\times 0.866$ for 2200 m/s value.

^bThermal self-shielding may be significant for Mn and Co.

^cNew thermal effect for copper (see text).

^dSee Table IV for gradients; 316 SS = Fe(.645), Ni(.13), Cr(.18), Mn(.019), Mo(.026).

Table IV. Helium and Displacement Damage for 316 SS* for RB2

Helium includes ⁵⁹Ni and fast reactions
DPA includes extra thermal kick (He/567)

<u>Height, cm</u>	<u>ne, appm</u>	<u>DPA</u>
0	1448	10.76
3	1432	10.65
6	1386	10.36
9	1306	9.85
12	1194	9.15
15	1052	8.24
18	880	7.16
21	679	5.88
24	457	4.40

*316SS: Fe(.645), Ni(.13), Cr(.18), Mn(.019), Mo(.026)

8.0 Publications

Two papers were presented at the International Conference on Nuclear Data for Basic and Applied Science in Santa Fe, NM., on May 13-17, 1985. One is listed as reference 3. The other is, as follows:

L. R. Greenwood and R. K. Smither, "New Neutron Cross Sections for Fusion Materials Studies," to be published.

HELIUM PRODUCTION IN COPPER BY A THERMAL THREE-STAGE REACTION

D. W. Kneff (Rockwell International), L. R. Greenwood, and E. L. Callis (Argonne National Laboratory)

1.0 Objective

The objectives of this work are to apply radiometric plus helium accumulation neutron dosimetry to the measurement of neutron fluences and energy spectra in mixed-spectrum fission reactors utilized for fusion materials testing, and to measure helium generation rates of materials in these irradiation environments.

2.0 Summary

The three-stage reaction process in copper that has been found to produce significant helium concentrations at high thermal neutron fluences has been analyzed in detail. Cross sections have been deduced for four reactions that allow us to calculate the total ${}^4\text{He}$ production in copper for high-fluence irradiations in the High Flux Isotopes Reactor (HFIR).

3.0 Program

Title: Helium Generation in Fusion Reactor Materials/Dosimetry and Damage Analysis

Principal Investigators: D. W. Kneff, H. Farrar IV, and L. R. Greenwood

Affiliation: Rockwell International and Argonne National Laboratory

4.0 Relevant DAFS Program Plan Task/Subtask

Task II.A.1 Fission Reactor Dosimetry

Task II.A.4 Gas Generation Rates

Subtask 11.A.5.1 Helium Accumulation Monitor Development

5.0 Accomplishments and Status

5.1 Introduction

The interpretation of fusion materials experiments performed in mixed-spectrum fission reactors often depends on calculated helium production and displacement damage rates. Rockwell International and Argonne National Laboratory (ANL) are participating in a joint program to measure total ${}^4\text{He}$ production rates over the range of fission reactor neutron spectra and fluences used for fusion materials testing, and to use the results to integrally test helium production cross sections used in damage calculations. Previous work has shown that helium production in reactor-irradiated nickel can be predicted to within 10%, using a detailed characterization of the irradiation environment and current cross section evaluations.⁽¹⁾

Recent work with Ti, Fe, and Cu samples irradiated in the mixed-spectrum reactors HFIR and ORR (Oak Ridge Research Reactor) at Oak Ridge and in the Experimental Breeder Reactor-II (EBR-II) have shown large discrepancies between helium generation measurements and predictions.⁽²⁾ For copper, the ratio of measured-to-predicted helium increases steeply with fluence above a thermal neutron fluence of about 10^{22} n/cm^2 . This increase is attributed predominantly to a previously unrecognized three-stage reaction process in copper for thermal neutrons.^(2,3) We have now determined the cross sections for four neutron-induced reactions in copper that provide a basis for calculating this enhanced helium.

5.2 Reactor Characterization and Experimental Measurements

Experiments performed in ORR and HFIR cover the neutron fluence range $1.2\text{--}15 \times 10^{22} \text{ n/cm}^2$. The reactor neutron spectra and fluence distributions were characterized using the multiple-activation dosimetry technique.⁽⁴⁾ Multiple activation wires providing long-lived activities upon activation were irradiated and then gamma counted using Ge(Li) spectroscopy, with measured activities generally accurate to $\pm 1.5\%$. Long wires were segmented to determine flux gradients. The measured activities were used to adjust calculated neutron spectra for each irradiation using the computer code STAYSL.⁽⁵⁾ Typical spectra are given in Ref. 1. The adjusted thermal, resonance, and fast neutron fluxes have estimated accuracies of 5–10%, although the uncertainties are highly correlated so that integral quantities tend to be more accurate. One important discrepancy observed in the high-fluence activation data was the unexpectedly low ^{65}Zn activity from irradiated copper samples, which provided evidence for this copper three-stage reaction mechanism.

The neutron fluence and spectral information from each irradiation were used to calculate fast helium production in the constituent elements of materials of interest for fusion reactor applications. The predictions for HFIR-irradiated copper, bracketing the fluence range of fusion materials experiments CTR30, CTR31, and CTR32, are shown as the dashed line in Figure 1. These predictions are based on the ENDF/B-V Gas Production file.⁽⁶⁾ The fast neutron fluences are ~0.8 times the thermal fluences given in Fig. 1, and represent neutron energies $> 0.1 \text{ MeV}$.

Helium measurements were performed for in multiple copper samples from a total of 20 different locations in HFIR experiments CTR30, 31, and 32, and ORR experiments MFEZ, 4A2, and 4B.^(2,3) The measurements were performed using isotope-dilution gas mass spectrometry,⁽⁷⁾ with absolute uncertainties of $\pm 1\text{--}2\%$. The results for HFIR are presented in Figure 1. The calculated-to-experimental helium ratios (C/E) ranged from 0.63 to 0.19 for HFIR, while the lower-fluence ORR measurements gave a nearly constant C/E ratio of about 0.64. The HFIR data clearly indicate a large enhancement in helium production at high fluences.

5.3 Helium Production Mechanisms

The reaction channels affecting helium production in reactor-irradiated copper are summarized in Figure 2. The fast reactions $^{63}\text{Cu}(n,\alpha)$ and $^{65}\text{Cu}(n,\alpha)$ dominate at low neutron fluences. The following three-stage reaction becomes important at high thermal neutron fluences ($>10^{22} \text{ n/cm}^2$):

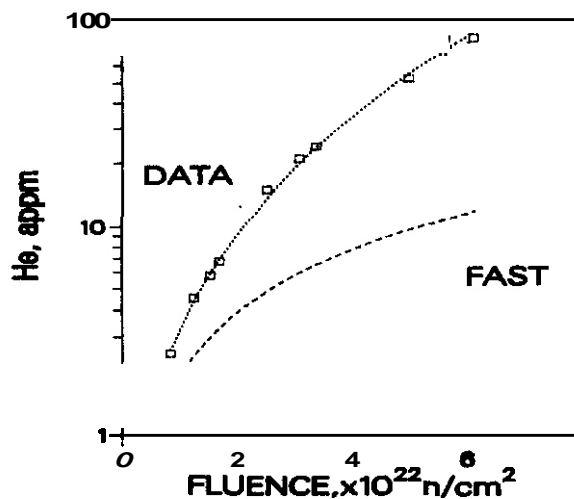
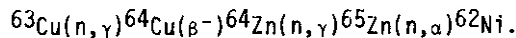


FIGURE 1. Measured and Predicted ^4He Production in Copper vs. Thermal Fluence for HFIR. The Dashed Line is the Fast ^4He Calculated from ENDF/B-V, Where the HFIR Fast Fluence ($>0.1 \text{ MeV}$) is ~ 0.8 Times the Thermal Fluence. The Line Through the Data is an Empirical Fit (see Discussion).

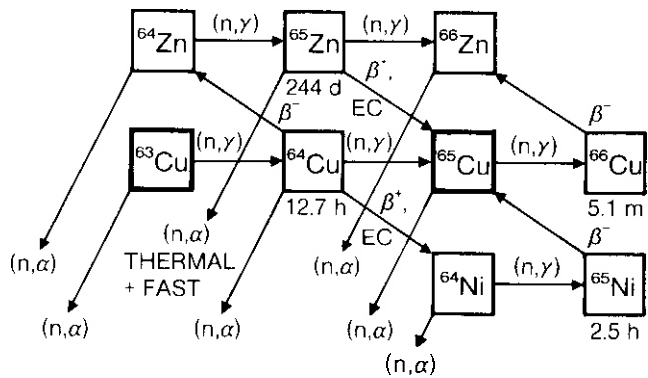


FIGURE 2. Reaction Channels Affecting ${}^4\text{He}$ Production in Copper.

TABLE 1
KNOWN NEUTRON CAPTURE CROSS SECTIONS USED IN THE COPPER CALCULATIONS

Reaction	Thermal Cross Section (barns)	Resonance Integral (barns)
${}^{63}\text{Cu}(n,\gamma){}^{64}\text{Cu}$	4.5	5.0
${}^{65}\text{Cu}(n,\gamma){}^{66}\text{Cu}$	2.17	2.19
${}^{64}\text{Zn}(n,\gamma){}^{65}\text{Zn}$	0.76	1.45
${}^{64}\text{Ni}(n,\gamma){}^{65}\text{Ni}$	1.52	0.98

Several other fast-neutron reactions also contribute at high fluences, but their net effect is not large. This includes, for example, the 2-stage reaction process ${}^{63}\text{Cu}(n,\gamma){}^{64}\text{Cu}(\beta^-){}^{64}\text{Zn}(n,\alpha){}^{61}\text{Ni}$. The reaction-chain ${}^{63}\text{Cu}(n,\gamma){}^{64}\text{Cu}(\beta^+){}^{64}\text{Ni}(n,\gamma){}^{65}\text{Ni}(\beta^-){}^{65}\text{Cu}(n,\alpha)$ produces only a negligible amount of ${}^4\text{He}$, but affects the ${}^{63}\text{Cu}/{}^{65}\text{Cu}$ isotopic ratio (see next section).

The accurate calculation of helium production through the three-stage process requires the knowledge of several reaction cross sections. Those that we consider to be well-known are summarized in Table 1. Three of the relevant thermal reaction cross sections are not well-known: ${}^{64}\text{Cu}(n,\gamma)$, ${}^{65}\text{Zn}(n,\text{abs})$ [$(n,\gamma)+(n,p)+(n,\alpha)$], and ${}^{65}\text{Zn}(n,\alpha)$. The spectrum-integrated (n,α) cross sections for fast neutrons are also generally not well-known, but can be calculated relative to the ${}^{63}\text{Cu}(n,\alpha)$ reaction for computational purposes. We have done so using the computer code THRESH2,(8) with the results given in Table 2. The fact that the lower-fluence ORR irradiations gave low, constant C/E ratios indicates that the spectrum-integrated ENDF/B-V evaluation for copper is low in this energy range.(2,3) ${}^{64}\text{Cu}(n,\alpha)$ was thus a fourth cross section to be measured.

5.4 Cross Section Measurements

The reaction mechanisms summarized in Figure 2 can be represented by 16 coupled differential equations, whose solutions provide final nuclear species ratios and ${}^4\text{He}$ reaction contributions for given irradiation conditions. The four unknown cross sections were determined by substituting a series of values into these equations to find the best fit to our experimental data.

The ${}^{64}\text{Cu}(n,\gamma){}^{65}\text{Cu}$ cross section was determined first, from the post-irradiation ${}^{65}\text{Cu}/{}^{63}\text{Cu}$ isotopic ratios. These ratios vary sensitively with neutron fluence at high fluences. They were measured experimentally by mass spectrometry for 9 copper samples which had been irradiated to different neutron fluences in three HFIR experiments. The results were compared with calculated ratios to determine the ${}^{64}\text{Cu}(n,\gamma)$ cross section that provided the best fit. The calculated ${}^{65}\text{Cu}/{}^{63}\text{Cu}$ ratios included the effects of ${}^{65}\text{Zn}$ decay and ${}^{64}\text{Ni}$ production and burnup to ${}^{65}\text{Cu}$. Our final ${}^{64}\text{Cu}(n,\gamma)$ cross section, 270 ± 170 mb, is sufficiently small that the large cross section uncertainty has a negligible effect on subsequent cross section determinations.

TABLE 2
 (n,α) CROSS SECTION RATIOS USED IN THE
 COPPER CALCULATIONS

Reaction	Ratio ^(a)
$^{63}\text{Cu}(n,\alpha)^{60}\text{Co}$	1
$^{64}\text{Cu}(n,\alpha)^{61}\text{Co}$	0.675
$^{65}\text{Cu}(n,\alpha)^{62}\text{Co}$	0.349
$^{64}\text{Zn}(n,\alpha)^{61}\text{Ni}$	2.365
$^{65}\text{Zn}(n,\alpha)^{62}\text{Ni}$	6.714
$^{66}\text{Zn}(n,\alpha)^{63}\text{Ni}$	1.238
$^{64}\text{Ni}(n,\alpha)^{61}\text{Fe}$	0.102

^(a)Ratios with respect to the reaction
 $^{64}\text{Cu}(n,\alpha)$, calculated using THRESH2,
 Ref. 8

The $^{65}\text{Zn}(n,\text{abs})$ thermal cross section was determined by fitting the measured ^{65}Zn reaction rates of 18 HFIR-irradiated samples. Our adopted value, 66 ± 8 barns, was then used in the determination of the thermal $^{65}\text{Zn}(n,\alpha)$ and fast $\text{Cu}(n,\alpha)$ cross sections. The $\text{Cu}(n,\alpha)$ fast helium production was separated from the enhanced helium (three-stage thermal process plus other multiple-step α -producing reactions) by varying both the $^{65}\text{Zn}(n,\alpha)$ cross section and the C/E fast helium ratio. The C/E ratio was used to calculate the fraction of the helium associated with the fast reactions. The high-fluence helium measurements in HFIR were dominated by the three-stage reaction, providing a relatively C/E-independent $^{65}\text{Zn}(n,\alpha)$ cross section measurement. At lower HFIR fluences the fast helium dominated, allowing the determination of the C/E ratio. Both values were determined from the best fit to the data over the total range of HFIR fluences. The ORK data were not included in these analyses because the dosimetry data indicated sufficient differences in the ORR and HFIR spectra to produce differing fast-neutron C/E ratios. Our deduced $^{65}\text{Zn}(n,\alpha)$ cross section is 4.7 ± 0.5 barns, and the C/E ratio deduced for fast helium production is 0.76. The latter gives a HFIR spectrum-integrated $\text{Cu}(n,\alpha)$ cross section of $313 \pm 20 \mu\text{b}$ for fast neutrons.

5.5 Discussion

The cross sections derived from the experimental data are summarized in Table 3. The uncertainties do not include the uncertainties associated with the cross sections and cross section ratios given in Tables 1 and 2, respectively, and may be quite sensitive to the capture cross sections. However, the present cross sections provide a consistent set for predicting ^4He generation for copper irradiated to high fluences in HFIR, based on data extending up to thermal neutron fluences of $6 \times 10^{22} \text{ neutrons/cm}^2$. These cross sections differ significantly from the corresponding ENDF/B-V cross sections, which are also listed in Table 3. For damage considerations, the three-stage mechanism produced 1 dpa (displacement per atom) for each 492 appm of helium. This is an insignificant fraction of the total dpa produced in copper at these HFIR fluences, in contrast to the significant damage produced by ^{59}Ni in the nickel two-stage reaction.⁽¹⁾

TABLE 3
 MEASURED HFIR CROSS SECTIONS

Reaction	Energy	Measured	ENDF/B-V ^(a)
$^{64}\text{Cu}(n,\gamma)^{65}\text{Cu}$	thermal ^(b)	$270 \pm 170 \text{ b}$	$<6000 \text{ b}$
$^{65}\text{Zn}(n,\text{abs})$ ^(c)	thermal ^(b)	$66 \pm 8 \text{ b}$	-
$^{65}\text{Zn}(n,\alpha)^{62}\text{Ni}$	thermal ^(b)	$4.7 \pm 0.5 \text{ b}$	$250 \pm 150 \text{ b}$
$\text{Cu}(n,\alpha)$	fast ($>0.1 \text{ MeV}$)	$313 \pm 20 \mu\text{b}$	$238 \mu\text{b}$

^(a)Ref. 6

^(b)Measured values include effects from a 7% epithermal flux

^(c) $(n,\gamma)+(n,p)+(n,\alpha)$

The following empirical expression, based on the measured helium concentrations, can be used to estimate the enhanced helium production:

$$\text{Enhanced } {}^4\text{He (appm)} = 0.669 \cdot \Phi^{2.58}$$

Here Φ is the thermal neutron fluence in units of 10^{22} n/cm^2 . This fit has a standard deviation of less than 7%. The total helium production in HFIK-irradiated copper is then determined by adding the fast-neutron contribution, when the latter is corrected for the 24% underprediction by ENDF/B-V.

6.0 References

1. L. R. Greenwood, D. W. Kneff, R. P. Skowronski, and F. M. Mann, "A Comparison of Measured and Calculated Helium Production in Nickel Using Newly Evaluated Neutron Cross Sections for ^{59}Ni ," J. Nucl. Mater., 122 & 123, 1002 (1984).
2. See, for example, D. W. Kneff, B. M. Oliver, R. P. Skowronski, and L. R. Greenwood, "Helium Production in Reactor-Irradiated Copper and Titanium, and Evidence for a Copper Three-Stage Reaction," in Damage Analysis and Fundamental Studies, Quarterly Progress Report October-December 1984, DOE/ER-0046/20, U.S. Department of Energy, 13 (1985).
3. D. W. Kneff, B. M. Oliver, and K. P. Skowronski, "Helium Production in Reactor-Irradiated Copper," in Damage Analysis and Fundamental Studies, Quarterly Progress Report January-March 1985, DOE/ER-0046/21, U.S. Department of Energy, 37 (1985).
4. L. R. Greenwood, "Neutron Flux and Spectral Measurements to Characterize Irradiation Facilities for Fusion Materials Studies," in Radiation Metrology Techniques, Data Bases, and Standardization, F. ti. K. Kam, Ed., Proc. Fourth ASTM-EURATOM Symposium on Reactor Dosimetry, Gaithersburg, Maryland, March 22-26, 1982, NUREG/CP-0029, U.S. Nuclear Regulatory Commission, 783 (1982).
5. F. G. Perey, "Least-Squares Dosimetry Unfolding: The Program STAY'SL," ORNL/TM-6062, Oak Ridge National Laboratory (1977); modified by L. R. Greenwood (1979).
6. ENDF/B-V Gas Production file for Cu, Mat 5329, by C. Y. Fu, Oak Ridge National Laboratory (1979).
7. B. M. Oliver, J. G. Bradley, and H. Farrar IV, "Helium Concentration in the Earth's Lower Atmosphere," Geochim. Cosmochim. Acta, 48, 1759 (1984).
8. S. Pearlstein, "Neutron Cross Sections and Their Uncertainties Obtained from Nuclear Systematics," in Nuclear Cross Sections and Technology, Vol. I, K. A. Schrake and C. D. Bowman, Ed., NBS Special Publication 425 (1975) pp. 332-333.

7.0 Future Work

Work is in progress to measure the total helium production cross sections of new materials that have been, and will be, irradiated in mixed-spectrum reactor experiments. The results will be used to test gas production cross section files and to improve helium generation predictions for fusion materials irradiations.

8.0 Publications

A paper entitled "Helium Production in Copper by a Thermal Three-Stage Reaction," by D. W. Kneff (Rockwell), L. R. Greenwood (ANL), B. M. Oliver, R. P. Skowronski (Rockwell), and E. L. Callis (ANL), was presented at the Int'l. Conf. on Nuclear Data for Basic and Applied Science, in Santa Fe, New Mexico in May 1985, and was submitted for publication in Radiat. Effects.

ON ISOTOPIC ALLOYING TO TAILOR HELIUM PRODUCTION RATES IN MIXED SPECTRUM REACTORS

L. K. Mansur, A. F. Rowcliffe, M. L. Grossbeck, and R. E. Stoller (Oak Ridge National Laboratory)

1.0 Objective

The purposes of this work are to increase the understanding of mechanisms by which helium affects microstructure and properties, to aid in the development of materials for fusion reactors, and to obtain data from fission reactors in regimes of direct interest for fusion reactor applications.

2.0 Summary

Isotopic alloying is examined as a means of manipulating the ratio of helium transmutations to atom displacements in mixed spectrum reactors. The application explored is based on artificially altering the relative abundances of the stable isotopes of nickel to systematically vary the fraction of ^{58}Ni in nickel-bearing alloys. The method of calculating helium production rates is described. Results of example calculations for proposed experiments in the High Flux Isotope Reactor are discussed.

3.0 Program

Title: Radiation Effects Mechanisms
Principal Investigator: L. K. Mansur
Affiliation: Oak Ridge National Laboratory

4.0 Relevant DAFS Program Plan/Subtask

Subtask II.C.2 Effects of Helium on Microstructure
Subtask II.C.8 Effects of Helium and Displacements on Fracture

5.0 Accomplishments and Status

5.1 Introduction

An important aspect of research into the effects of irradiation on structural materials at elevated temperatures is the interaction of transmutation-produced helium with displacement damage. Helium is an insoluble inert gas typically produced to levels of a few tenths appm/dpa in fast reactor irradiations and to levels of up to tens of appm/dpa in fusion reactor environments. It has been found that this gas may produce significant changes in dimensional stability and mechanical properties of structural materials [1,2], and may strongly affect microstructural development and phase stability [3].

In planned fusion reactors, the 14 MeV component of the (D,T) fusion neutron spectrum ensures the simultaneous production of displacement damage and high helium concentrations in materials used for the first wall, the blanket structure, and related components of a fusion reactor. Until a 14 MeV neutron machine suitable for fusion materials research is constructed, materials scientists must utilize fission reactors and accelerators to investigate radiation damage effects and to develop improved materials. In order to study the effects of helium, several approaches have been developed and used with varying degrees of success. Dual-ion beam irradiations, in which a self-ion beam of the material in question is used to produce displacements and a helium ion beam is used to inject the gas, provide an excellent means of exploring the influence of helium on microstructural evolution over a very wide range of He:dpa ratios [4]. This technique is a powerful means of exploring radiation damage mechanisms in both simple and complex alloys. For metals and simple binary or ternary alloys it is possible to predict many aspects of in-reactor microstructural development when the effects of high damage rate, injected interstitials, diffusional spreading and surface proximity are accounted for [5]. However, in complex structural alloys, the prediction of in-reactor behavior from heavy-ion experimental data is confounded by complex precipitation reactions that are temperature and dose rate dependent.

A second approach to the investigation of helium effects is to introduce helium into the material either by cyclotron injection or by the diffusion of tritium followed by radioactive decay to ${}^3\text{He}$. The helium-bearing materials are subsequently irradiated in a fast reactor to produce displacement damage. These techniques are applicable to a wide range of materials and have been used to explore the influence of

helium on both microstructural evolution [6] and on mechanical properties [7,8]. The primary disadvantage of this approach is that the helium and displacement damage are not generated simultaneously.

A third approach to studying helium effects which is limited to nickel-bearing alloys, is to irradiate in mixed-spectrum fusion reactors. Here the fast neutron component of the spectrum produces high levels of damage, accompanied by some transmutation products including helium, while the thermal and epithermal component of the neutron spectrum produces high levels of helium by the two-step reaction [9]



Here, however, the helium can achieve levels many times that expected in fusion reactors, depending on the dose and on the nickel content of the specific alloy in question. For example, for stainless steels with nickel contents in the range of about 15%, the helium concentration is of the order of 10,000 appm at 100 dpa for irradiations in the High Flux Isotope Reactor at Oak Ridge National Laboratory. This is five to ten times the He:dpa ratio expected in fusion reactors. For alloys that contain less nickel, the correspondence is better. To isolate the effects of helium on microstructural evolution and swelling, the same material is irradiated in a fast reactor where the helium production rate is several tens of appm per dpa. This approach is expensive, since it requires two reactor irradiations, and frequently the comparison of data from two reactors is compromised by differences in temperature history, neutron spectra, and damage levels.

Helium generation rates in nickel-bearing alloys may also be varied during irradiation in a mixed-spectrum reactor by using the spectral tailoring technique [10]. Here the local neutron spectrum is modified by surrounding the irradiation capsule with the appropriate thermal neutron absorbers, and the nickel two-step transmutation reactions [Eq. (1)] are controlled at the required rates. This is a powerful technique for irradiating nickel-bearing alloys at the correct He:dpa ratio for fusion reactor applications. To isolate specific phenomena attributable to helium, comparison irradiations are required either in the same reactor without thermal neutron absorbers (higher helium) or in a fast reactor (lower helium).

The purpose of the present work is to examine an approach which allows the helium generation rate to be varied widely in alloys of identical chemical composition, during side-by-side irradiation in a mixed-spectrum reactor. We term the method isotopic alloying and for the present consider only applications to nickel-bearing alloys, although this kind of approach is also applicable to other alloy systems. Since ${}^{58}\text{Ni}$ is responsible for high-helium production, the idea is to systematically deplete or enrich it in favor of other stable isotopes of nickel, while maintaining the overall nickel chemical composition constant. This approach will, for the first time, permit in-reactor experiments in which the main variable is the helium generation rate, thus improving the quality of mechanistic studies. It also provides a means of assessing the response of developmental alloys to high levels of displacement damage with the simultaneous generation of helium at rates appropriate for a fusion reactor experiment.

In the next section we present an analysis for isotopic alloying in general. Following this, example results for the High Flux Isotope Reactor (HFIR) at Oak Ridge National Laboratory are presented. Included are calculations covering several experiments. This is followed by a discussion and summary, where various classes of experiments that can be investigated by isotopic alloying are suggested.

5.2 Analysis

5.2.1 General

It is sufficient for present purposes to consider that each isotope may produce helium by both thermal and epithermal neutron reactions on the one hand and by fast neutron reactions on the other hand. Therefore we may write

$$n = n_t + n_f = \sum_e \sum_i (p_{\ell}^i + s_{\ell}^i) q_{\ell}^i r_{\ell} , \quad (2)^*$$

*Equation (2) is a simplification of the more general form containing multiple neutron groups, $n =$

$\sum_m \sum_i p_{\ell,m}^i q_{\ell,m}^i r_{\ell}$, where now $p_{\ell,m}^i$ is the helium generating function for isotope i of element ℓ applicable to neutron energy group m .

where n is the number of helium atoms per atom of alloy, and t denotes time. The quantities $n_t = \sum_i p_i q_i r_i$ and $n_f = \sum_a \sum_i s_i q_i r_i$ are the fractional helium levels produced by thermal and fast reactions, respectively. Hence p_i and s_i are the helium generating functions for thermal and fast reactions giving the cumulative number of helium atoms produced per initial atom of isotope i of element ℓ at time t . Expressions for these helium generating functions typically are obtained either by derivation considering the physics of the particular nuclear reactions in question or by empirical fits to measured helium production data. The symbol q_ℓ^i is the initial fraction of atoms of isotope i of element ℓ to all atoms of element ℓ in the alloy, and r_ℓ is the atom fraction of element ℓ in the alloy, so that $\sum_i q_\ell^i = \sum_\ell r_\ell = 1$.

The quantities q_ℓ^i are of primary interest here. The crux of isotopic alloying is to manipulate q_ℓ^i at will, not simply accepting the naturally occurring distribution of stable isotopes. This manipulation may be accomplished by combining more than one isotopic mixture of element ℓ . For example, we might make use of the naturally occurring mixture and one or more mixtures enriched or depleted in an isotope of interest. The mixtures are combined in various proportions to achieve systematic variations. In general, q_ℓ^i is given by

$$q_\ell^i = \sum_j a_{j,\ell}^i b_{j,\ell} . \quad (3)$$

Here $a_{j,\ell}^i$ is the atom fraction of isotope i in the isotopic mixture j of element ℓ . Similarly, $b_{j,\ell}$ is the atom fraction that isotope mixture j comprises of total atoms of element ℓ of the alloy. Again, $\sum a_{j,\ell} = \sum b_{j,\ell} = 1$.

The above is cast all in terms of atom fractions. When specifications are in terms of weight fractions, the necessary conversions are made prior to using Eqs. (2) and (3). Instead of $a_{j,\ell}$, $b_{j,\ell}$ and r_ℓ , consider that the specifications $w_{j,\ell}^i$, $x_{j,\ell}$ and y_ℓ now denote respectively the weight fraction of isotope i in mixture j of element ℓ , the weight fraction of isotope mixture j to total element ℓ , and the weight fraction of element ℓ to the total alloy. Letting m_ℓ^i denote the atomic mass of isotope i of element ℓ , we define the following quantities:

$$\bar{m}_{j,\ell} = (\sum_i w_{j,\ell}^i / m_\ell^i)^{-1} , \quad (4)$$

$$\bar{m}_\ell = (\sum_j x_{j,\ell} / \bar{m}_{j,\ell})^{-1} , \quad (5)$$

and

$$\bar{m} = (\sum_\ell y_\ell / \bar{m}_\ell)^{-1} . \quad (6)$$

The quantity $\bar{m}_{j,\ell}$ is the average atomic mass of isotopes of element ℓ in mixture j , \bar{m}_ℓ is the average atomic mass of isotopes of element ℓ in the alloy and \bar{m} is the average atomic mass of all isotopes of all elements in the alloy. From these we obtain $a_{j,\ell}^i$, $b_{j,\ell}$ and r_ℓ for use in Eqs. (2) and (3) as follows,

$$a_{j,\ell}^i = w_{j,\ell}^i \bar{m}_{j,\ell} / m_i^\ell , \quad (7)$$

$$b_{j,\ell} = x_{j,\ell} \bar{m}_\ell / \bar{m}_{j,\ell} \quad (8)$$

$$r_\ell = y_\ell \bar{m}_\ell / \bar{m}_\ell . \quad (9)$$

5.2.2 Alloys Containing Nickel

In many structural materials for applications, where the effects of helium are of interest, the main alloying constituents are Fe, Cr, Ni, Mn, Mo, Ti, Nb, V, Al, Cu, and V. For these, because the fast neutron cross-sections are low, helium production from fast neutron reactions is adequately represented by the simple expression neglecting isotopic depletion

$$s_\ell^i = \sigma_{\ell,He}^i \phi t , \quad (10)$$

where $\sigma_{\ell,He}^i$ is the spectral-averaged helium production cross-section of isotope i of element ℓ for one-step (n,α) reactions and ϕ is the total neutron flux. The corresponding function p_ℓ^i for helium production from thermal neutron reactions is taken to be negligible for all isotopes except for ^{58}Ni .** Thus, all p_ℓ^i in Eq. (2) are neglected, except p_{Ni}^{58} . Therefore n_t becomes $p_{\text{Ni}}^{58} q_{\text{Ni}}^{58} r_\ell$.

Production of helium from ^{58}Ni proceeds with high cross-sections via the two-step reaction described by Eq. (1). The function p_{Ni}^{58} for this case is obtained from the classical equations of nuclide buildup and decay [12,13]. For the interested reader, the equations are obtained as follows. At time t' the fraction of ^{58}Ni remaining is given by $e^{-\sigma_Y \phi t'}$, where σ_Y is the spectral-averaged (n,γ) cross-section. In the time interval between t' and $t'+dt'$, therefore, the fraction $e^{-\sigma_Y \phi dt'} \sigma_Y \phi dt'$ ^{59}Ni atoms will be formed, while the fraction of these persisting until time t is $e^{-\sigma_T \phi (t-t')}$. Here σ_T is the total neutron absorption cross-section of ^{59}Ni . The fraction of ^{59}Ni existing at fluence ϕt , designated as f' , is therefore the integral of these incremental contributions

$$f' = \sigma_Y \int_0^{\phi t} e^{-\sigma_Y \phi t'} e^{-\sigma_T \phi (t-t')} \phi dt' , \quad (11)$$

leading to

$$f' = \frac{\sigma_Y}{\sigma_T - \sigma_Y} (e^{-\sigma_Y \phi t} - e^{-\sigma_T \phi t}) . \quad (12)$$

Similarly, if f' is the fraction of ^{59}Ni existing at fluence $\phi t'$, then $f' \sigma_T \phi dt'$ is the fraction of ^{59}Ni that is transformed to other species in the fluence interval between $\phi t'$ and $\phi t' + \phi dt'$. Thus the cumulative fraction of ^{59}Ni transformed at fluence ϕt , designated as f , is

$$f = \frac{\sigma_Y}{\sigma_T - \sigma_Y} \int_0^{\phi t} (e^{-\sigma_Y \phi t'} - e^{-\sigma_T \phi t'}) \sigma_T \phi dt' \quad (13)$$

$$f = \frac{\sigma_T (1 - e^{-\sigma_Y \phi t}) - \sigma_Y (1 - e^{-\sigma_T \phi t})}{\sigma_T - \sigma_Y} \quad (14)$$

The quantity p_{Ni}^{58} is simply the fraction of transformed ^{59}Ni that has taken the (n,α) route, i.e.,

**

Recently, some evidence has been presented that isotopes of Cu may lead to small but non-negligible helium production in a thermal neutron three-step reaction [11].

$$p_{Ni}^{58} = f \frac{\sigma_\alpha}{\sigma_T}, \quad (15)$$

where σ_α is the spectral-averaged (n, α) cross-section of ^{59}Ni .

Before describing results for helium buildup in specific alloys, it is useful to record some properties of these functions. For high fluence, i.e., $\phi t \gg \frac{1}{\sigma_T}$, f approaches unity as expected. On the other hand as $\phi t \rightarrow 0$, $f \rightarrow \sigma_T \sigma_Y (\phi t)^2/2$. This behavior results from the fact that the concentration of target species, ^{59}Ni , is linear with fluence at low fluences and that the concentration of the product species, α or ^{56}Fe , is linear in the target species and in fluence, so that at low fluences the helium concentration is quadratic with fluence. The derivative of f' with respect to $\sigma_T \phi t$, designated as f''^* and given by

$$f''^* = \frac{\sigma_Y/\sigma_T}{\sigma_T - \sigma_Y} (\sigma_T e^{-\sigma_T \phi t} - \sigma_Y e^{-\sigma_Y \phi t}), \quad (16)$$

is also useful. The fluence where $f''^* = 0$ gives the maximum in f' . It also gives the inflection point in f . Thus this fluence determines the maximum value of ^{59}Ni attainable and simultaneously gives the point beyond which helium accumulation is less than linear with fluence and prior to which helium accumulation is greater than linear with fluence. Setting $f''^* = 0$ yields this fluence as

$$(\phi t)^* = \ln(\sigma_T/\sigma_Y)/(\sigma_T - \sigma_Y). \quad (17)$$

For example, using spectral-averaged cross-sections appropriate to the HFIK PTP position [14] gives $(\phi t)^* \approx 9.4 \times 10^{26} n/m^2$ total fluence. Table 1 gives the spectral-averaged cross-sections.

Table 1
Spectral-averaged total cross-sections for the HFIR PTP [13].

Cross-section	Value (barns)
σ_Y	1.615
σ_α	4.292
σ_T	34.00

The functions f , f' , and f''^* are plotted in Figure 1 for the HFIR PTP spectral-averaged cross-sections. In Figure 1(a) is shown f . This is the shape of the He accumulation function by slow neutron reactions that arises in all subsequent calculations for specific alloys. At a total fluence of $2 \times 10^{28} n/m^2$ the helium accumulation is only a few percent from saturation (unity). To obtain the helium accumulated per initial atom of ^{58}Ni , this function need only be multiplied by σ_α/σ_T or 0.126 for the present values. Figure 1(b) shows f' . This gives directly the fraction of ^{59}Ni to initial ^{58}Ni at any fluence. For the current cross-section values, the peak value of ^{59}Ni is about 4% at the value of $(\phi t)^*$. Figure 1(c) shows the behavior of f''^* .

5.3 Applications

We have recently obtained a special isotopic mixture of nickel that is highly enriched in ^{60}Ni (99.65%). The atomic composition of this mixture is given in Table 2 together with that of naturally occurring nickel. A batch of ^{58}Ni of similar purity has also been obtained from the Operations Division of Oak Ridge National Laboratory and is included in the table. Using these isotopes, we envisage pursuing two broad categories of experiments using the HFIK target region irradiation facilities.

1. Experiments which are formulated on the basis of radiation effects theory and mechanisms, and which address fundamental aspects of helium effects in nickel-bearing alloys.
2. Experiments designed to assess the response of nickel-bearing structural alloys to the high levels of displacement damage and helium expected in a fusion reactor environment. The ability to reproduce these aspects of the fusion neutron environment is crucial to alloy development activities involving a wide range of physical and mechanical property measurements.

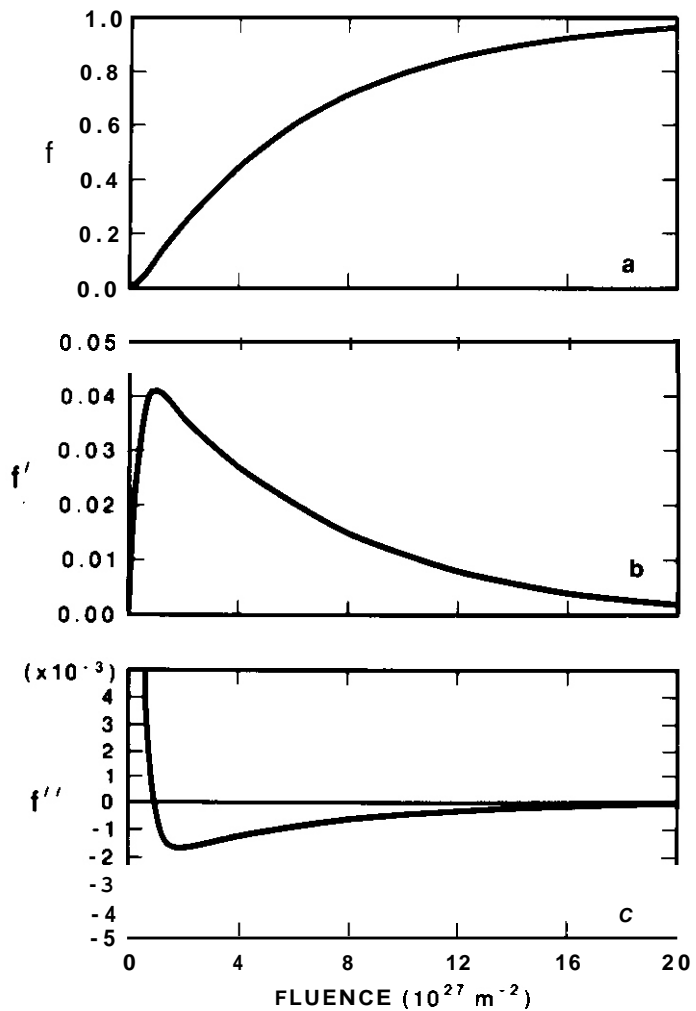


Fig. 1. The functions f , f' , and f'' versus fluence for a wide range of fluence. The cumulative fraction (f) of ^{59}Ni to initial ^{58}Ni transformed to other species (a), the instantaneous fraction (f') of ^{59}Ni (b), and (f'') its derivative (c).

Table 2
Isotopic compositions (%) of nickel isotope mixtures.

Mixture	^{58}Ni	^{60}Ni	^{61}Ni	^{62}Ni	^{64}Ni
Natural	68.3	26.1	1.1	3.6	0.9
Special ^{60}Ni	U.29	99.65	0.03	0.03	<0.008
Special ^{58}Ni	99.875	U.093	0.005	0.008	-0.019

Both of these types of experiments, mechanistic and scoping, could also be carried out with materials that do not normally contain nickel, but to which nickel is added to increase helium production. It then becomes additionally necessary to determine the effects of the nickel addition on the basic physical metallurgy of the alloy system. Examples of these various types of experiments are outlined in the following.

The first example is based on an experiment to investigate the onset of swelling. It utilizes a set of Fe-35Ni-15Cr and Fe-15Ni-15Cr alloys with different levels of ^{58}Ni . The background to this experiment is as follows. In earlier work [15], we compared swelling in these alloys under ion irradiation. We found that swelling began later and was lower at any dose in the Fe-35Ni-15Cr alloy, thus confirming earlier observations [16]. The behavior was understood in terms of a recently developed theoretical concept — that

swelling is triggered when a critical number of gas atoms is accumulated in a cavity [17]. It was found that the 35Ni alloy required a much larger critical number of gas atoms and correspondingly had a larger critical cavity radius than the 15Ni alloy. To further test the theory, we propose to irradiate both the 35Ni and 15Ni alloy in HFIR in several versions possessing identical chemical compositions but where the fraction of ^{58}Ni is varied by isotopic alloying. The idea is that the required critical number of gas atoms to initiate swelling would remain identical in alloys of the same chemical composition, but that the critical number would be achieved at different fluences, depending on the helium production rate dictated by isotopic alloying. Thus, the onset of swelling will be determined by the initial ^{58}Ni level if the theory is correct.

The helium accumulation in the Fe-35Ni-15Cr alloy is shown in Figure 2. Figure 2(a) gives results for q_{Ni}^{58} ranging from 0.613 (natural nickel) to 0.071 (1 part natural nickel and 9 parts special ^{60}Ni inixture).

Figure 2(b) shows the results for $q_{\text{Ni}}^{58} = 0.0029$ (i.e., all nickel is from the special ^{60}Ni mixture). This gives the minimum achievable helium level in this alloy in the HFIR PTP region. Fast neutron reactions lead to a significant fraction of the helium in Fig. 2(b) (~40%). We see that more than a factor of 50 difference in helium levels is achievable (more than 70 if $q^{58} \leq 1$, as in the special ^{58}Ni inixture). Correspondingly, we expect a large difference in the fluences at which the accumulation of the critical number of gas atoms is achieved.

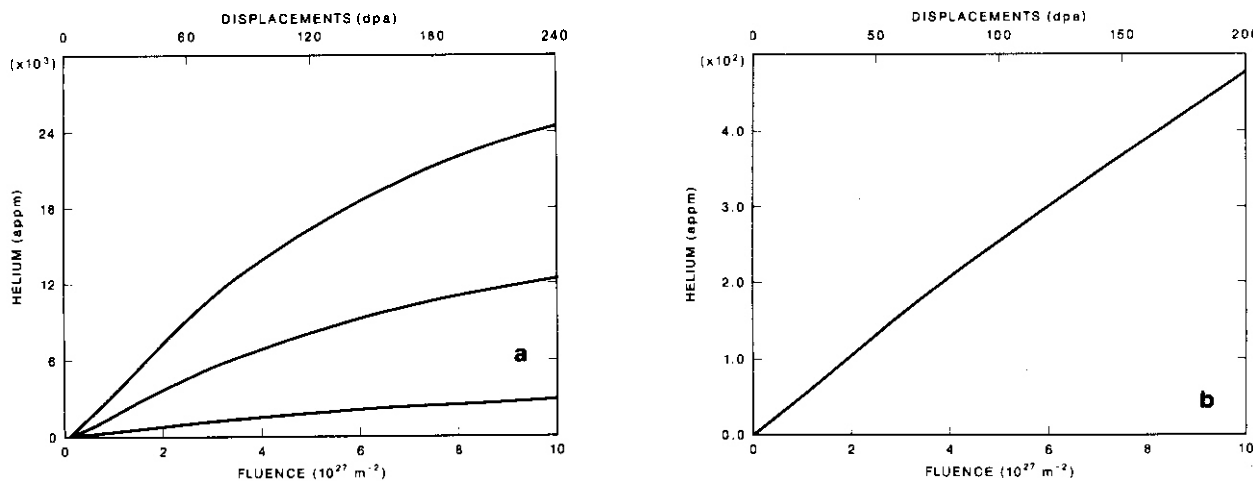


Fig. 2. Calculated helium accumulation in the alloy Fe-35Ni-15Cr in the HFIR PTP versus fluence and displacements. Part (a) shows the results for q_{Ni}^{58} of 0.683 (natural nickel) 0.343 and 0.071, and part (b) shows the results for q_{Ni}^{58} of 0.0029. The displacement scale applies only to the upper curve in part (a), because of the additional displacements produced by the ^{56}Fe recoils.

A related experiment would examine the influence of the He/dpa ratio on cavity density. The results of many dual and triple ion irradiation studies and a limited amount of fission reactor data indicate that the cavity density may exhibit a simple power dependence on the He/dpa ratio: i.e. $N_c \propto (He/dpa)^p$, where p is in the range of 0.25 to 2 [18]. Determining the appropriate value of p for the much longer irradiation times in reactors would increase the usefulness of the large fission reactor swelling data base for predicting swelling in a fusion reactor environment. For low values of p , the higher fusion He/dpa ratio would be expected mainly to reduce the amount of time required for bubbles to acquire the critical number of gas atoms and hence reduce the time interval to the onset of bias-driven swelling. For high values of p , on the other hand, the increased cavity density could extend the incubation time by partitioning the helium to many more cavities and by increasing the overall point defect sink strength. These considerations have been explored previously [19], where the potential for a peak in swelling vs He/dpa ratio for values of the He/dpa ratio was indicated near the nominal level expected in a fusion reactor first wall. By varying the amount of ^{58}Ni in an alloy, He/dpa ratios can be obtained that bracket this value and provide the data necessary to determine the value of p .

In striving to tailor the He/dpa ratio by isotopic alloying, the additional damage caused by (n,α) reactions must be considered, as has been pointed out by Greenwood, et. al. [14]. In particular it has been shown that the ^{56}Fe recoils from the second step of the reaction of equation (1) may cause a significant number of displacements. The damage has a one-to-one correspondence with the helium produced; for

every 567 appm He one additional dpa is produced. Thus for the 35Ni alloy of Figure 2(a), at a fluence of $1 \times 10^{28} \text{ n/m}^2$ (~ 198 dpa) the additional damage would be approximately 42 dpa, giving a total damage level of ~ 240 dpa. On the other hand the effect is small in alloys containing only a few percent nickel.

Another example is the application of isotopic tailoring to study the mechanisms involved in high-temperature intergranular embrittlement — a radiation-induced phenomenon which afflicts a wide range of fcc structural alloys [20]. Present evidence suggests that matrix hardening, grain boundary segregation, precipitation, and bubble formation all contribute in some measure to intergranular separation at low ductility levels. However, it is not possible, in a single reactor experiment, to define the relative importance of these phenomena; progress in improving alloy properties has consequently been very limited. With isotopic alloying it becomes possible, in principle, to vary helium generation independently of the other microstructural changes which occur during irradiation. Figure 3 shows the helium production in HFIR for three chemically identical heats of an austenitic stainless steel designated PCA, based upon 14 wt % Cr–16 wt % Ni with q_{Ni}^{58} values of 0.683 (natural Ni), 0.071 (1 part natural Ni and 3 parts ^{60}Ni special mixture), and U.0029 (all ^{60}Ni special mixture). Thus, irradiation in the HFIR target region provides the opportunity to study the deformation behavior of metallurgically identical heats irradiated under identical conditions, the main variable being the three different levels of helium. Extensions of this approach to a further set of alloys modified with titanium would help to resolve some long-standing questions regarding the role of TiC particles in improving resistance to intergranular failure.

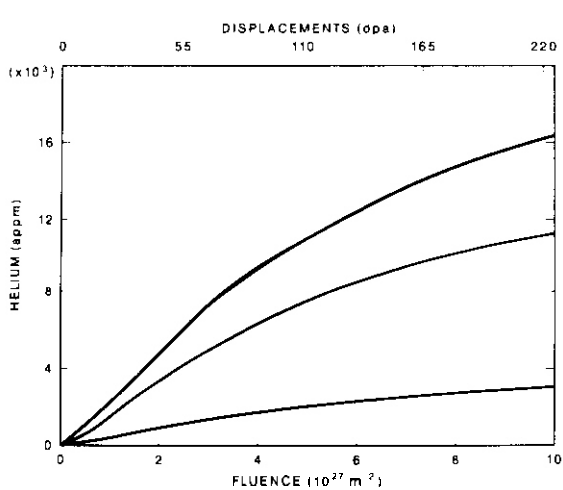


Fig. 3. Calculated helium accumulation in the 300 series stainless steel PCA for q_{Ni}^{58} of 1, 0.683, and 0.173. The displacement scale applies only to the upper curve because of the additional displacements produced by the ^{56}Fe recoils.

Other experiments using the isotopic tailoring method may be visualized in alloys that normally contain little or no nickel. To achieve levels of He:dpa ratio in the range of interest for fusion applications requires a few atomic percent nickel. However, the effects of nickel additions on the physical metallurgy of the alloy system need to be identified and accounted for. One way to do this is to prepare the alloy doped with ^{58}Ni for maximum helium generation and in addition to prepare control heats (a) doped with ^{60}Ni and (b) without any nickel added. Irradiation of the three alloys would allow unfolding of the helium effects from the compositional effects on alloy structure and properties.

An example of this type of experiment is with the 12Cr-1MoVW ferritic steel HT-9, which is of interest for fusion reactor applications. This alloy normally contains ~0.5 wt % Ni. Figure 4 shows the helium generation for alloys with $q_{\text{Ni}}^{58} = 1.0$ and 0.683. For an irradiation dose of 100 dpa, replacing the natural nickel with ^{58}Ni raises the helium concentration by 50% to ~400 at. ppm. When ^{58}Ni is maximally depleted (by doping with 0.5 wt % ^{60}Ni), the concentration of helium at 100 dpa drops to ~80 at. ppm. Side-by-side irradiation of these alloys in HFIR provides a means of investigating mechanisms associated with the migration, trapping, and precipitation of helium and the effects of helium on void nucleation and on the mechanical behavior of the tempered martensite structure. To assess the response of this alloy to the helium concentrations expected in a fusion reactor, it is necessary to increase the ^{58}Ni concentration to ~1.5 wt % to produce ~1200 at. ppm at 100 dpa. To this end, we have already carried out an extensive investigation of the effect of adding natural nickel concentrations in the range 1 to 2 wt % on the tempering response, tensile, and impact properties, and long-term thermal stability of both 9Cr and 12Cr

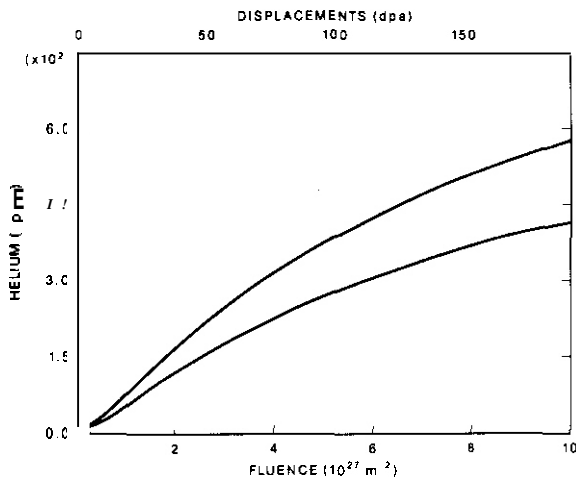


Fig. 4. Calculated helium accumulation in the alloy HT-9 for q_{Ni}^{58} of 1 and 0.683.

martensitic steels [21]. With this knowledge of the physical metallurgy of the nickel-doped steels, we should be able to separate the irradiation-induced property changes due to nickel from those associated with helium generation.

5.4 Related Experiments

Recently a related idea to that presented here has been proposed [22,23]. The purpose would be to reproduce the He:dpa ratio appropriate to a fusion reactor in a fission reactor using nickel-bearing alloys doped with ^{59}Ni . The approach differs from that described in the present paper, and is more complex and expensive. The ^{59}Ni would be obtained by first irradiating nickel in a mixed-spectrum reactor. In the approach of de Raedt, the ^{59}Ni would be generated by first irradiating either the specimen or nickel feedstock in a thermal neutron flux. The pre-irradiated specimens, or new specimens prepared from the nickel containing ^{59}Ni , would then be irradiated in a harder neutron spectrum to produce helium. In the method suggested by Simons, the nickel containing ^{59}Ni would be used to prepare specimens that could be then irradiated in a mixed-spectrum reactor (HFIR) or a fast-spectrum reactor (FFTF). An advantage of ^{59}Ni doping in alloys to be irradiated in a mixed-spectrum reactor is that the low helium production rate phase early in dose [see our discussion following Eq. (15), and Fig. 1], where ^{59}Ni is being built up, could be eliminated. Fast-reactor irradiations would be accomplished in relatively soft spectrum locations to induce the necessary helium transmutation rates in the ^{59}Ni -containing alloys. To make the most use of this approach the ^{59}Ni , an unstable isotope with a half-life of about 7.5×10^4 years, should be separated from the remaining nickel to allow flexible admixtures for alloying. Handling, separation, and alloy melting using radioactive materials are needed to use this method. When ^{59}Ni is added initially to an alloy, then Eq. (2) contains a corresponding new term of the form $p_{\text{Ni}}^{59}q_{\text{Ni}}^{59}r_{\text{Ni}}^{59}$. Here $p_{\text{Ni}}^{59} = (1 - e^{-5T\phi t})\sigma_{\alpha}/\sigma_T$ and q_{Ni}^{59} designates the fraction that ^{59}Ni initially comprises of total nickel.

The use of Ni isotopes is only one example of isotopic alloying to enhance helium generation during irradiation. Clinard [24] has pointed out that isotopic tailoring with other elements may be used to study the effects of helium and hydrogen generation on the behavior of ceramics during irradiations. Doping with ^{170}W would enhance helium generation in a mixed-spectrum reactor by the thermal neutron reaction $^{170}\text{W}(n,\alpha)^{14}\text{C}$, while the addition of ^{14}N would generate hydrogen through the $^{14}\text{N}(n,p)^{14}\text{C}$ reaction. In these cases, however, the reaction product may be a foreign element in the material, unlike the ^{56}Fe in Fe-Ni-Cr base alloys.

5.5 Conclusions

Isotopic alloying using naturally occurring stable isotopes is a means to manipulate the ratio of helium transmutation to atom displacement rates in mixed-spectrum reactors. The application examined is to nickel-bearing alloys, where the two-step reaction of Eq. (1) produces up to about 0.13 helium atoms to each initial atom of ^{58}Ni . The method proposed is to systematically vary the fraction of ^{58}Ni to total Ni, by admixtures of naturally occurring nickel with special mixtures depleted or enriched in ^{58}Ni .

A method is described to calculate helium levels produced by neutron transmutation reactions in any material. This is applied to nickel bearing alloys in mixed-spectrum reactors. Results of example calculations are described for irradiations in the High Flux Isotope Reactor at Oak Ridge National Laboratory.

Three types of experiments can be identified where isotopic alloying would be useful for research in radiation effects. These relate to studies of mechanisms, to applied research for fusion reactor applications, and to novel experiments to encompass alloys that do not normally contain nickel. The first type of experiment addresses the physical bases of helium effects and may be formulated based on the theory of radiation effects. The second type aims to characterize helium effects in parameter regimes and materials of direct interest for fusion reactor applications. The novel experiments involve introducing nickel to produce helium in materials that do not normally contain nickel. Both isotopic controls containing the same fraction of nickel but depleted in ^{58}Ni , and compositional controls containing no nickel are to be irradiated simultaneously. Thus the effects of helium on the material should be separable from the effects of nickel on the physical metallurgy of the alloy systems.

6.0 References

1. J. S. Whitley, K. L. Wilson, and F. W. Clinard, Jr., Proc. of the Third Topical Meeting on Fusion Reactor Materials, Albuquerque, September 1983, J. Nucl. Mater. **122&123** (1983).
2. Proc. Int'l. Symposium on Fundamental Aspects of Helium in Metals, Rad. Effects **78** (1983).
3. K. Farrell, P. J. Maziasz, E. H. Lee, and L. K. Mansur, p. 277 in Ref. [2].
4. G. Ayrault, H. A. Hoff, F. V. Nolfi, and A. P. L. Turner, J. Nucl. Mater. **103&104** (1981) 1035.
5. L. K. Mansur and M. H. Yoo, J. Nucl. Mater. **85&86** (1979) 523.
6. P. J. Maziasz, J. Nucl. Mater. **108/109** (1982) 359.
7. D. G. Alteridge, A. S. Johnson, L. A. Charlot, J. F. Remark, and R. E. Westerman, "Effects of Helium Implanted by Tritium Decay on High Temperature Mechanical Properties of Niobium," Proc. Int'l. Conf. on Radiation Effects and Tritium Technology for Fusion Reactors, Gatlinburg, TN, Oct. 1-3, 1975, CONF--750989, Vol. 11, pp. 307-330.
8. D. N. Braski and D. W. Ramey, "A Modified Tritium Trick Technique for Doping Vanadium Alloys with Helium," ASTM STP **870**, 1985, pp. 1211-1224.
9. J. Weitman, N. Daverhög, and S. Farvolden, Trans. Amer. Nucl. Soc. **13** (1970) 557.
10. R. L. Klueh and E. E. Bloom, Nucl. Eng. and Design **73** (1982) 101.
11. D. W. Kneff, B. M. Oliver, R. P. Skowronski, and L. R. Greenwood, U.S. Department of Energy Damage Analysis and Fundamental Studies Quarterly Progress Report, February 1985, DOE/ER-0046/20.
12. R. D. Evans, "The Atomic Nucleus," McGraw-Hill Book Company, New York, 1955, p. 477.
13. L. R. Greenwood, D. W. Kneff, R. P. Skowronski, and F. M. Mann, J. Nucl. Mater. **122&123** (1984) 1002.
14. L. R. Greenwood, U.S. Department of Energy Damage Analysis and Fundamental Studies Quarterly Progress Report, August 1983, DOE/ER-0046/14.
15. E. H. Lee and L. K. Mansur, "Evidence for a Mechanism of Swelling Variation in Irradiated Fe-Cr-Ni Alloys, Phil. Mag. (in press).
16. W. G. Johnston, J. H. Rosolowski, A. M. Turkalo, and T. Lauritzen, J. Nucl. Mater. **54** (1974) 24.
17. For a review, see L. K. Mansur and W. A. Coghlan, J. Nucl. Mater. **119** (1983) 1.
18. G. R. Odette, P. J. Maziasz, and J. A. Spitznagel, J. Nucl. Mater. **103&104** (1981) 1289-1304.
19. R. E. Stoller and G. R. Odette, "Effects of Radiation on Materials," ASTM STP **782** (1982) 275-294.
20. D. R. Harries, J. Nucl. Mater. **82** (1979) 2-21.
21. R. L. Klueh, J. M. Vitek, and M. L. Grossbeck, "Nickel-Doped Ferritic Steels for Fusion Reactor Irradiation Studies: Tempering Behavior and Tensile Properties," ASTM STP **782**, 1982, 648-664.

22. Ch. De Raedt. Proc. Conf. on Fast, Thermal and Fusion Reactor Experiments, April 1982, Salt Lake City, Utah, American Nuclear Society, p. 2-336.
23. R. L. Simons, U.S. Department of Energy Damage Analysis and Fundamental Studies Quarterly Progress Report, February 1983, DOE/ER-0046/12.
24. F. W. Clinard, Jr., J. Nucl. Mater. 85&86 (1979) 393.

7.0 Future Work

Two isotope mixtures enriched in ^{58}Ni and ^{60}Ni have been urucured from the ORNL Isotopes Program and planning *is* underway for the experiments described in the text. Details of the experiments will be described in a future report.

CHAPTER 3

REDUCED ACTIVATION MATERIALS

ACTIVATION CALCULATIONS WITH AN EXPANEO CROSS-SECTION LIBRARY

D. G. Doran and F. M. Mann (Hanford Engineering Development Laboratory)

1.0 Objective

The objective of this work is to calculate with reasonable accuracy and completeness the activation and transmutations that elements in fusion reactor first wall components will experience.

2.0 Summary

The activation of a number of elements has been calculated for 10 and 40 MW-y/m² at a STARFIRE first wall location using a greatly expanded cross-section library and multiple time steps. The results for critical radioisotopes (those that lead to concentration limits to meet low level radwaste criteria) are consistent at the lower fluence with earlier work , and found to increase nearly linearly with fluence.

3.0 Program

Title: Irradiation Effects Analysis

Principal Investigator: D. G. Doran

Affiliation: Hanford Engineering Development Laboratory

4.0 Relevant Program Plan Task/Subtask

No tasks on reduced activation were identified in the original DAFS Program Plan.

5.0 Accomplishments and Status

5.1 Introduction

The activation of elements at a fusion reactor first wall have been calculated at this laboratory by Mann⁽¹⁾ , and at other laboratories. These calculations are generally incomplete because their associated cross section libraries are incomplete, multi-step reactions may be excluded or treated only crudely, and high fluence effects may be inferred incorrectly from low fluence results. Each of these problem areas is being addressed in the present work. A further complication is accounting adequately for the sensitivity of the results to the neutron spectrum. This question was addressed in a previous publication⁽²⁾ in which the activation in several conceptual reactors was compared. It was found that the STARFIRE spectrum was generally the most severe, because the low energy tail produced by the water coolant, combined with I^{135} (n,γ) cross sections, resulted in large spectral-averaged cross sections. Therefore, the STARFIRE first wall spectrum was selected for the present study.

An expanded cross section library has been created by Mann for use with his REAC code.⁽³⁾ It contains cross sections for at least 14 reactions for each of 337 isotopes--6000 reactions in all. The goal was completeness. In order to achieve it, many reaction cross sections had to be approximated. This point is emphasized because it is easily forgotten when viewing tables of numbers generated by the code. We propose to evaluate only those cross sections, if any, that lead to unacceptable uncertainties in the calculated activation of critical radioisotopes. A critical radioisotope is defined as one that may lead to a concentration limit on an element in order to satisfy criteria for low level radwaste, recycling, maintenance, etc.⁽⁴⁾

The calculations were carried to 40 MW-y/m^2 , an early lifetime goal of the fusion program for first wall materials. The development of materials that can tolerate extremely high doses is still considered a desirable goal in light of the trend toward higher wall loadings. Composition changes due to transmutations can become extensive; they are calculated in REAC along with the activation.

The calculations were performed in steps of 1 MW-y/m^2 , or 0.277 years, at 3.6 MW/m^2 wall loading. Decay was followed after 10 and 40 MW-y/m^2 . For some reactions [notably (n,γ)] having large cross sections, even this step size is too large to yield high accuracy.

This is a progress report of a reexamination of the elements studied by Mann (1) to determine the effects of the extended cross section library, multiple time steps, and higher fluence. The calculations have been completed and are still being analyzed, but some general results of interest have been obtained.

5.2 Results

The results obtained to date can be summarized as follows:

1. The activated isotopes resulting from the irradiation of a single element of atomic number Z ranged from $Z=8$ to $Z+6$. An example is shown in Fig. 1.

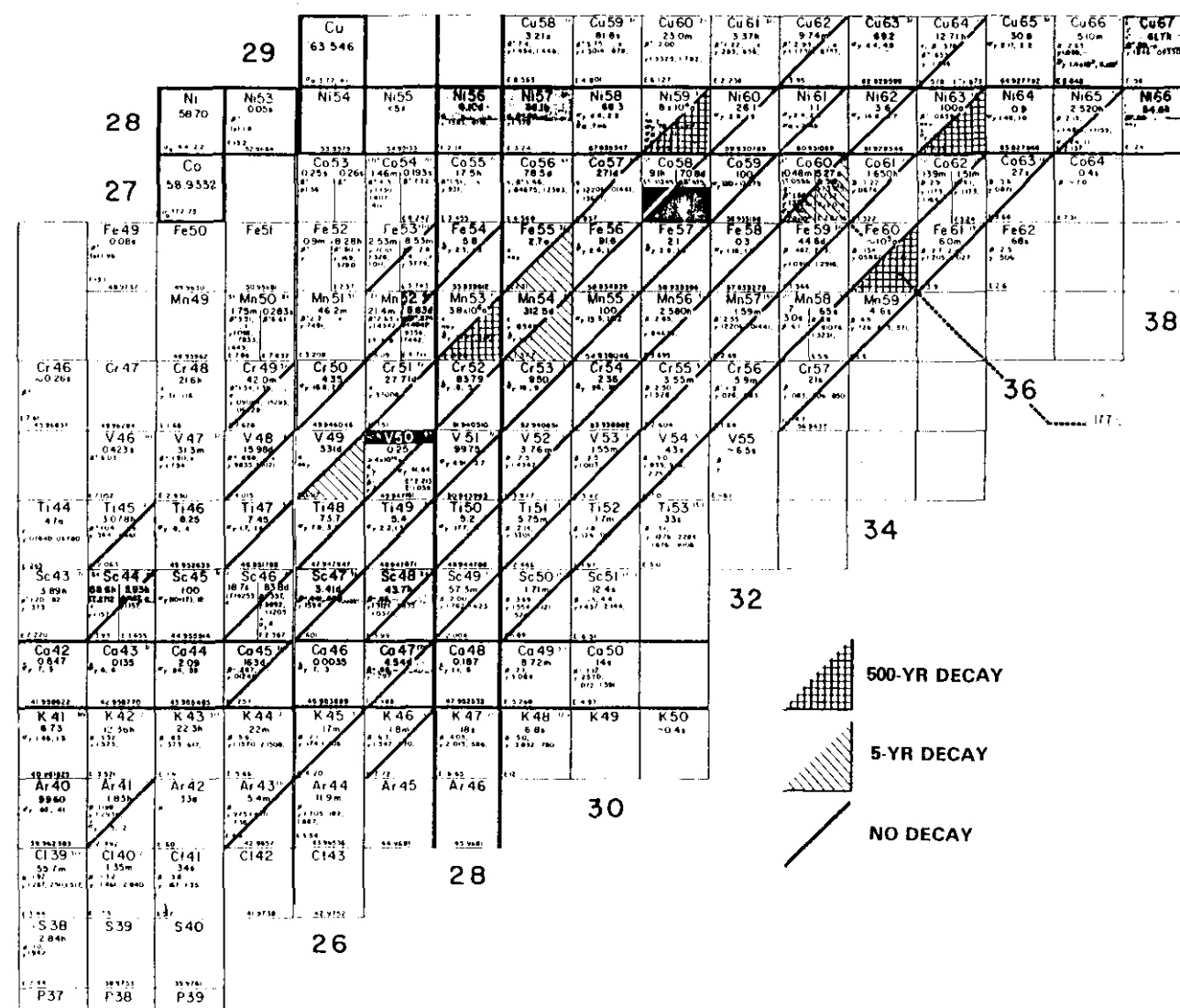


FIGURE 1. Significant Isotope Production When Pure Iron is Irradiated to 40 MW-yr/m^2 at STARFIRE First Wall

2. The activation of long-lived radioisotopes was generally consistent with Ref.1. No significant new activities were revealed for the major components of common structural materials.
3. The long-lived activity of an element after 40 MW-y/m² was often less than 4 times the activity after 10 MW-y/m² due to burnout effects. There are notable exceptions; e.g., for Ta the factor was 1000. For the elements identified in Ref. 1 as having concentration limits under Class C waste criteria, the factor ranges between 1.2 and 6, as is shown in Table 1.
4. New activation values for Co, Zr, Sn, Hf, and W may lead to concentration limits to satisfy class C waste criteria after both 10 and 40 MW-y/m². Titanium and Ta may also have limits after the higher fluence.
5. The activation after short-to-intermediate decay times of V, Zr, Nb, and Sn was much higher than found in Ref.1. This may be significant when the potential for recycling materials is examined.
6. Transmutation rates can be very high in the STARFIRE spectrum. An exposure of 40 MW-y/m² in STARFIRE, corresponding to a fluence of $6.4 \times 10^{23} \text{ n/cm}^2$, essentially eliminates Ta, and transmutes over half of W and Co and about one-quarter of Mn, Nb, and Hf. At 10 MW-y/m², Ta and W are about two-thirds and one-quarter transmuted; Co, Mn, and Hf are in the 5-10% range. High Z elements (above Mo) generally transmute to higher Z elements through (n,gamma) reactions, whereas lower Z elements generally produce transmutation products having both higher and lower Z.

6.0 References

1. F. M. Mann, Fusion Technol. 6, 273 (1984).
2. H. L. Heinisch and F. M. Mann, "A Comparison of Activation in STARFIRE and MARS First Walls", OAFS Quarterly Progress Report DOE/ER-0046/15, Nov. 1983, p.40.
3. F. M. Mann, "Cross Sections for Reduced Activation Studies", OAFS Quarterly Progress Report, DOE/ER-0046120, Feb. 1985, p. 18.
4. D. G. Doran, H. L. Heinisch, and F. M. Mann, "Reduced Activation Guidelines in Perspective", OAFS Quarterly Progress Report, DOE/ER-0046/19, Nov. 1984, p.24.

TABLE 1
COMPARISON OF ACTIVATION OF CRITICAL ISOTOPES AT TWO EXPOSURES

ORIGINAL ELEMENT	ACTIVATED ISOTOPE	<u>40 MW-y/10 MW-y*</u>
N	C-14	3.6
Al	Al-26	3.8
Ni	Ni-63	3.8
cu	Ni-63	6.0
Nb	Nb-94	1.2
Mo	Mo-93	2.7
	Nb-91	2.8
	Tc-99	3.5
Pb	Pb-205	3.6

*Ratio of activation at 40 MW-y/m² to that at 10 MW-y/m²

7.0 Future Work

Analysis of the REAC runs will be completed and results reported quantitatively for both activation and transmutation.

8.0 Publications

1. F. M. Mann, H. L. Heinisch, and D. G. Doran, "HEOL Reduced Activation Analysis: Status Report", Trans. ANS **49**, 66 (1985).
2. H. L. Heinisch, F. M. Mann, and D. G. Doran, "Spectral Dependence of Activation at Fusion Reactor First Walls", to be published in Fusion Technology.
3. D. G. Doran, H. L. Heinisch, and F. M. Mann, "Reduced Activation Guidelines in Perspective", in Proceedings of First International Conf. on Fusion Reactor Materials, Tokyo, Dec. 1984; to be published in J. Nucl. Mat.
4. F. M. Mann, D. E. Lessor, and J.S. Pintler, "REAC Nuclear Data Libraries", in Proceedings of International Conf. on Nuclear Data for Pure and Applied Sciences, Santa Fe, N. M., May 1985; to be published in Radiation Effects.
5. E. T. Cheng, J. A. Blink, B. A. Engholm, F. M. Mann, and A. M. White, "Uncertainties in Fusion Nuclear Waste Calculations", Trans. ANS **49**, 67 (1985).

CHAPTER 4

RADIATION EFFECTS MECHANISMS AND CORRELATIONS

THE MICROSTRUCTURAL EVOLUTION OF HEAVY-ION-IRRADIATED HT-9 FEKRITIC STEEL EXAMINED IN CROSS SECTION

J.J. Kai, G.L. Kulcinski and R.A. Dodd (University of Wisconsin-Madison)

1.0 Objective

The purpose of this study is to understand the microstructural/microchemical evolution of HT-9 ferritic steel under heavy ion irradiation.

2.0 Summary

A set of irradiated HT-9 specimen were examined by using a newly developed cross-section technique. The specimens were irradiated with 14 MeV Ni⁺³ ions in the temperature range from 300°C to 600°C and to the peak damage level of 200 dpa.

After irradiation at 300°C/400°C, the microstructure consisted of a high density of dislocation loops. After 500°C irradiation, a few large dislocation loops and a group of new precipitates, which were identified as chi phase were the major microstructural features. After irradiation at 600°C, no significant damage was found which indicated that thermal effects dominated the microstructural evolution at this temperature and above.

3.0 Program

Title: Radiation Effects to Reactor Materials
Principal Investigators: G.L. Kulcinski and R.A. Dodd
Affiliation: University of Wisconsin-Madison

4.0 Relevant OAFS Program Task/Subtask

Subtask II.C.1.1 Phase Stability Mechanics
Subtask II.C.6.1 Effect of Uamage Rate on Microstructural Evolution

5.0 Accomplishments and Status

5.1 Introduction

In this study, a set of HT-9 specimens that were irradiated with 14 MeV Ni⁺³ ions at temperatures of 300°C, 400°C, 500°C, and 600°C up to a peak damage level of 200 dpa were examined in cross-section. The cross-section technique has been described previously.¹ With some changes, the success percentage of this technique was improved from about 50% up to nearly 100%. The procedures of this newly improved cross-section technique were described in Reference 2.

The advantage of examining an ion irradiated specimen in cross-section is that the whole range of the damage and the control region can be seen in one specimen, so that the effects of radiation, dose rate, and dose

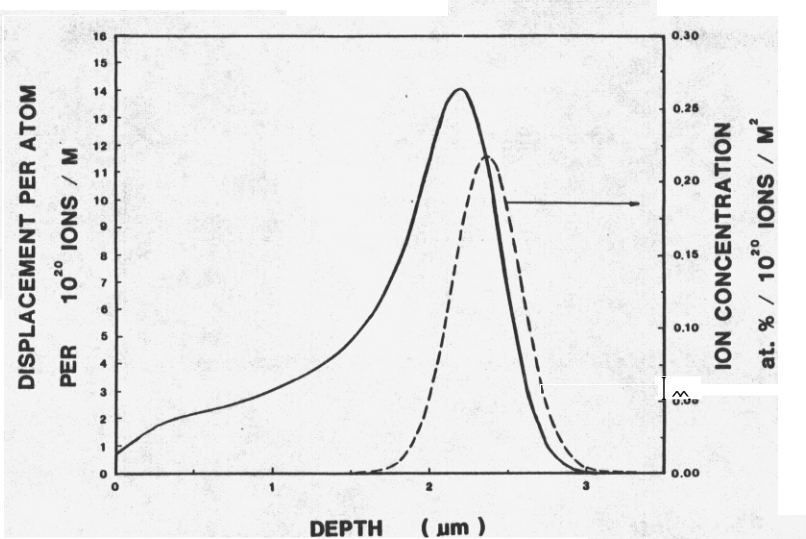


FIGURE 1. The dpa and deposition vs. depth curves of 14 MeV Ni ion on HT-9 targets.

level can be viewed simultaneously. Furthermore, the microstructural evolution in the damage region and the control region can be directly compared.

5.2 Experimental Procedures

The irradiation experiments were performed in a tandem Van de Graff Accelerator³ with a SNICS type negative ion source.⁴ The irradiation temperatures were accurate to $\pm 5^\circ\text{C}$. Three dose levels were achieved: 3×10^{20} , 8×10^{20} , and 15×10^{20} ions/ m^2 which are equivalent to about 40 dpa, 100 dpa and 200 dpa respectively at the damage peak and about 10 dpa, 25 dpa and 50 dpa respectively at the 1 μm depth.

The TEM analyses were performed in a JEOL 200 CXII TEM/SCAN microscope.

5.3 Results

The calculated dpa and ion deposition distribution versus depth curves of 14 MeV Ni⁺² ions injected into HT-9 are shown in Figure 1. Figures 2 and 3 show the TEM microstructures of HT-9 specimens irradiated at 300°C for total ion fluences of 3×10^{20} ions/ m^2 and 8×10^{20} ions/ m^2 , respectively. A very high number density of black spots is the major microstructural feature. From the enlarged micrograph, it is clear that these black spots are actually small dislocation loops. The nature of these loops has not been identified due to the present lack of AMG pole piece on the JEOL 200CX TEM.

The average size of the loops seems independent of the dose level and is about 10 nm in diameter. The number density of the loops saturates at higher dose levels.

Figures 4 and 5 show the microstructures of specimens irradiated at 400°C and total fluences of 3×10^{20} ions/ m^2 and 8×10^{20} ions/ m^2 , respectively. The basic structure in the irradiated regions is very similar to the 300°C case, except that the dislocation loops have larger average size of about 30 nm. Just as in the 300°C case, the size of the loops is independent of the dose level and the number density of the loops saturates at higher dose levels.

In the enlarged portion of Figure 5, it can be clearly seen that there are some very small (5 - 10 nm in diameter) black spots which are believed to be a new type of precipitate. This new phase has not yet been

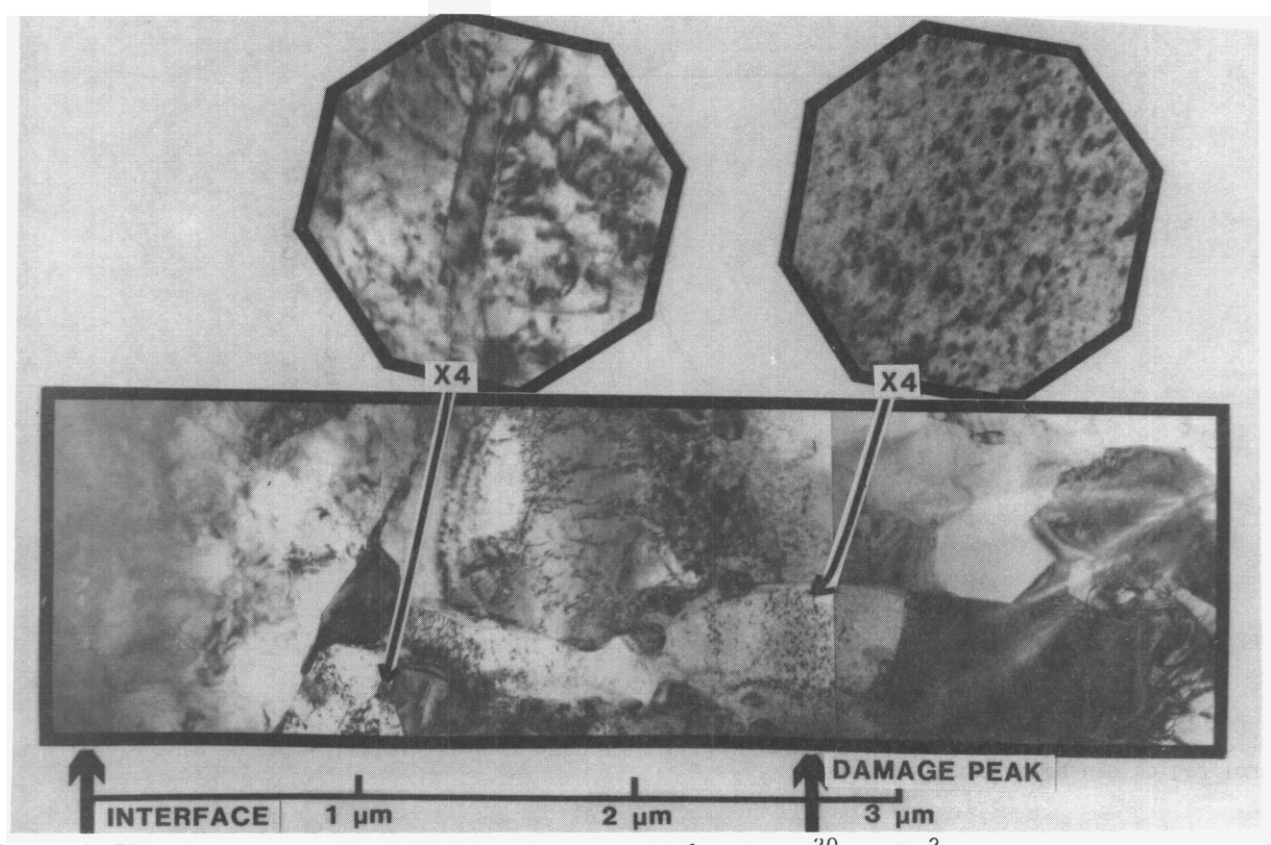


FIGURE 2. TEM microstructures of HT-9 irradiated at 300°C. 3×10^{20} ions/ m^2 .

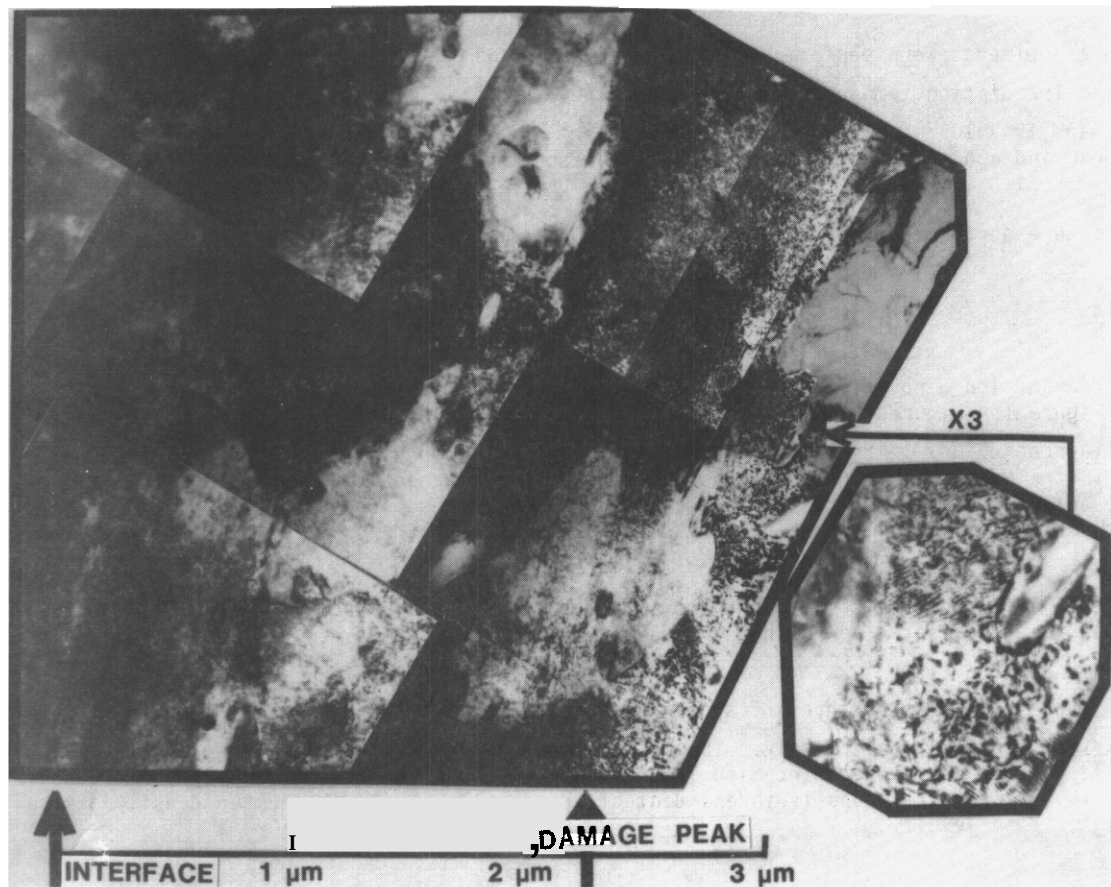


FIGURE 3. TEM microstructures of HI-9 irradiated at 300°C, 8×10^{20} ions/ m^2 .

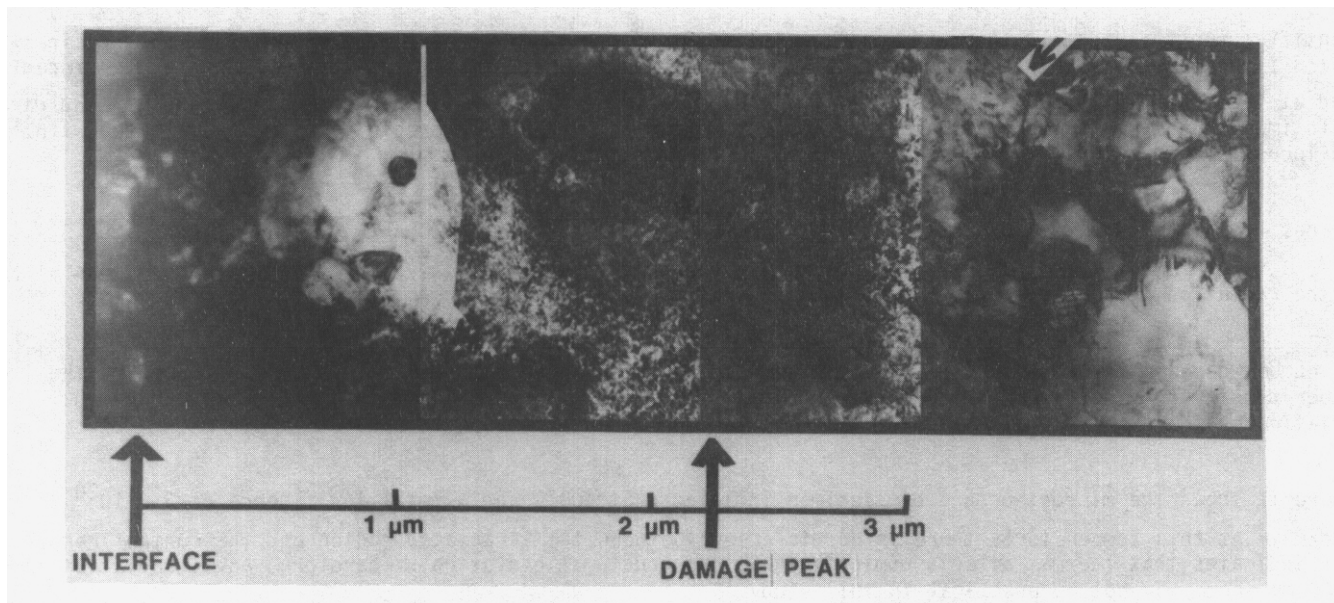


FIGURE 4. TEM microstructures of HT-9 irradiated at 400°C, 3×10^{20} ions/m².

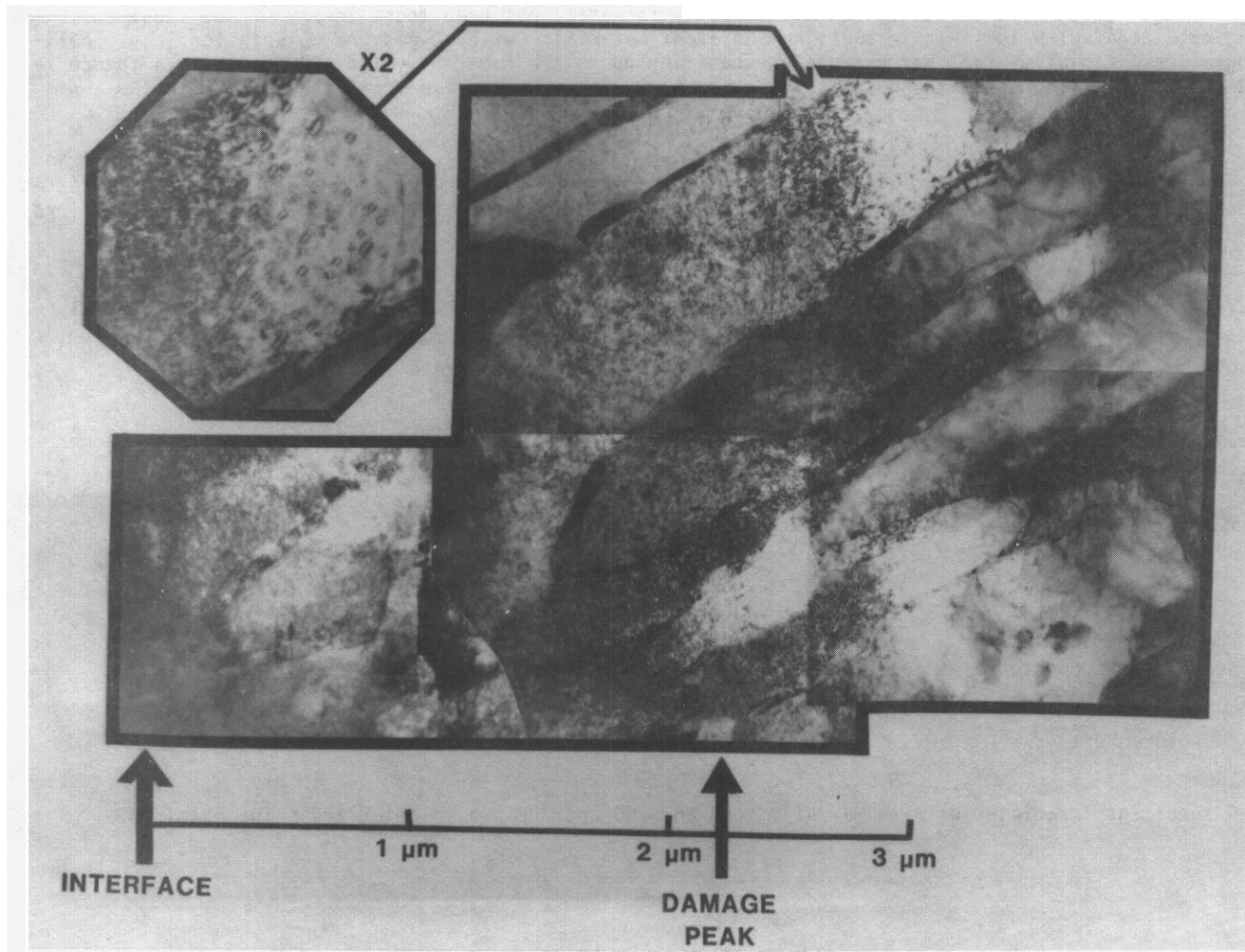


FIGURE 5. TEM microstructures of HT-9 irradiated at 400°C, 8×10^{20} ions/m².

identified due to the small size. However, Little & Stow⁵ have found Cr-enriched α' phase in neutron irradiated iron-chromium alloys containing $\geq 10\%$ Cr which is very similar to the new phase found in HT-9 irradiated at 400°C. Therefore, the new phase is believed to be the α' phase. Figure 6 shows the bright and dark field images of a portion of the damage region. It shows that the small precipitates are correlated with the loops to some extent.

Figures 7, 8 and 9 show the microstructure of specimens irradiated at 500°C and total ion fluences of 3×10^{20} , 8×10^{20} and 14×10^{20} ions/m², respectively. As described previously,⁶ the microstructure consists of the radiation induced chi phase, some large loops (average diameter 80 nm) and dislocation segments.

The number density of loops and the dislocation density are independent of the dose level. However, the number density and the average diameters of chi phase do vary with different doses. Figure 10 show the variation of the number density and the average diameter versus the dose levels.

Figure 11 shows the microstructure of specimen irradiated at 600°C and a total ion fluence of 3×10^{20} ions/m². At this temperature, there is no difference between the irradiated region and the control region. This indicates that thermal effects dominate the microstructural evolution. Therefore, any irradiation at 600°C or above may not be practical in this study.

5.4 Discussion

One significant result of this study is that no cavity formation has been found in any of the specimens. This indicates that HT-9 is a highly swelling resistant material: without gas preimplantation. e.g., helium, single ion irradiation does not produce any cavities up to the damage level of 200 dpa. In a future report, the authors will present the results of cavity formation in heavy ion irradiated HT-9 with 100 appm preimplanted helium.

The chi phase formed in 500° irradiations is summarized in Figure 10. The size of the precipitate increases with dose and the number density decreases with dose. This indicates that the chi phase is induced by irradiation and continuously grows to larger particles with irradiation.

The qualitative results of loop analysis reveals that the size increases with temperature. Little et al.⁷ reported an opposite effect in a material similar to HT-9 (except with a small amount of Nb content), but this might be due to the mistaken identification of chi phase as dislocation loops.

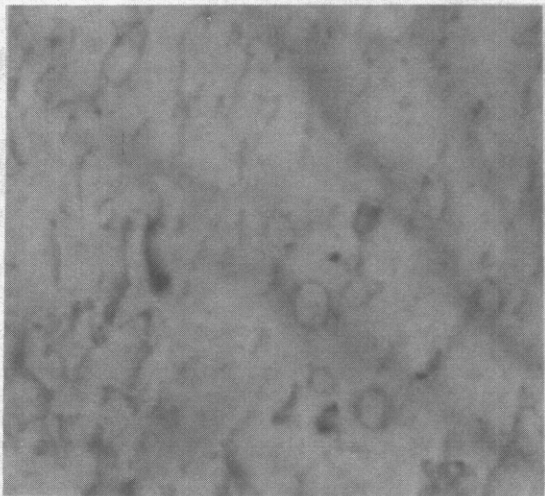
The precipitates found after the 400°C irradiations were too small to identify. However, Gelles & Thomas' reported α' phase in a study of neutron irradiated HT-9, as does Little & Stoter.⁹ Both of these studies strongly suggested that the new phase found in 400°C irradiations were the α' phase. More work is needed to identify this phase unambiguously.

6.0 Acknowledgements

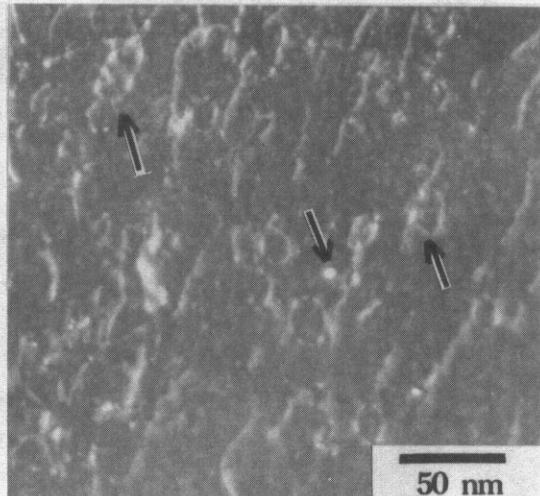
This research was supported by the U.S. Department of Energy, Office of Fusion Energy.

7.0 Future Work

The HT-9 specimens irradiated with 14 MeV Ni⁺³ ions and 100 appm He preimplanted are being examined.



BF



CDF

FIGURE 6. The small precipitates in damage region in HT-9 irradiated at 400°C.

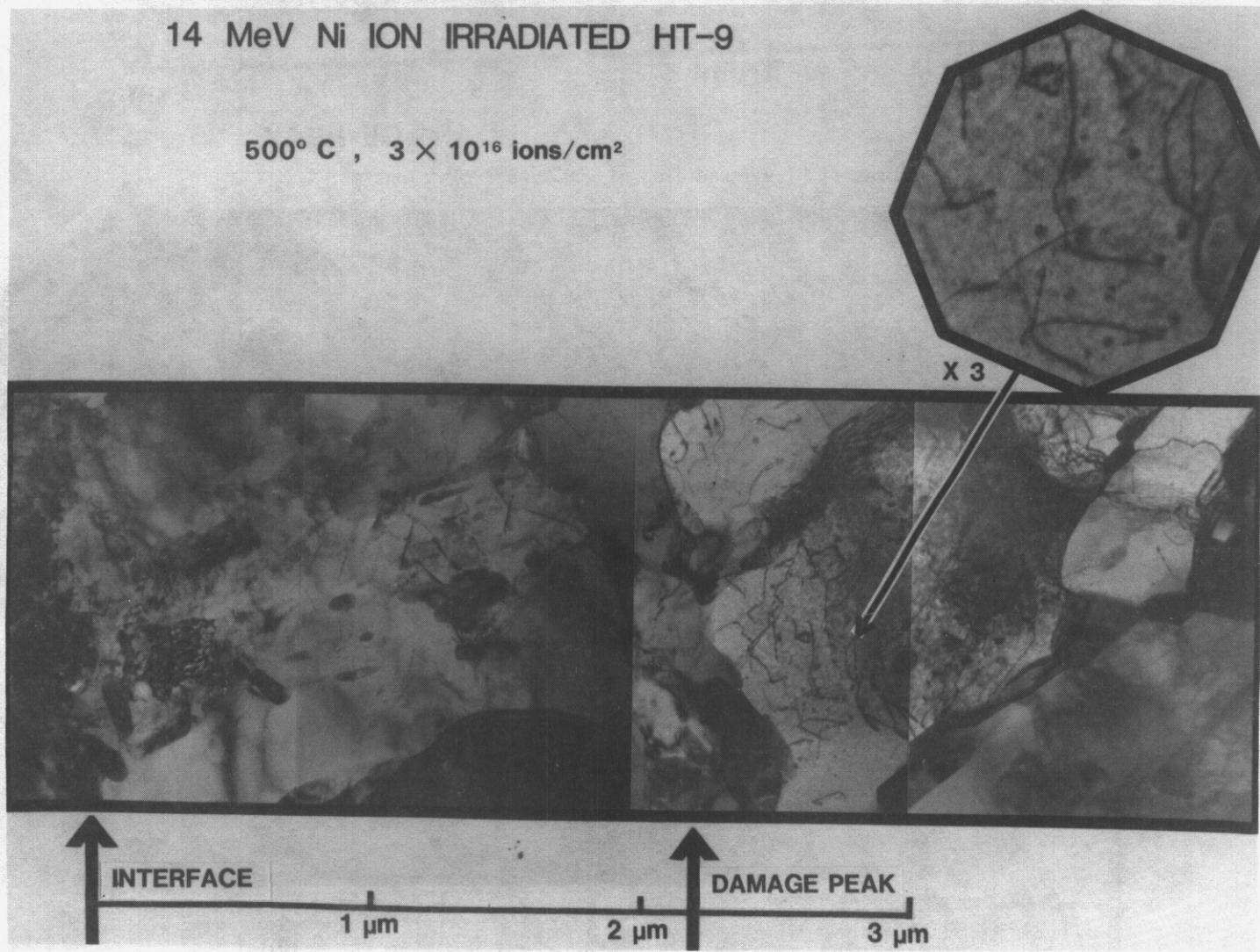


FIGURE 7. TEM microstructures of HT-9 irradiated at 500°C, 3×10^{20} ions/m².

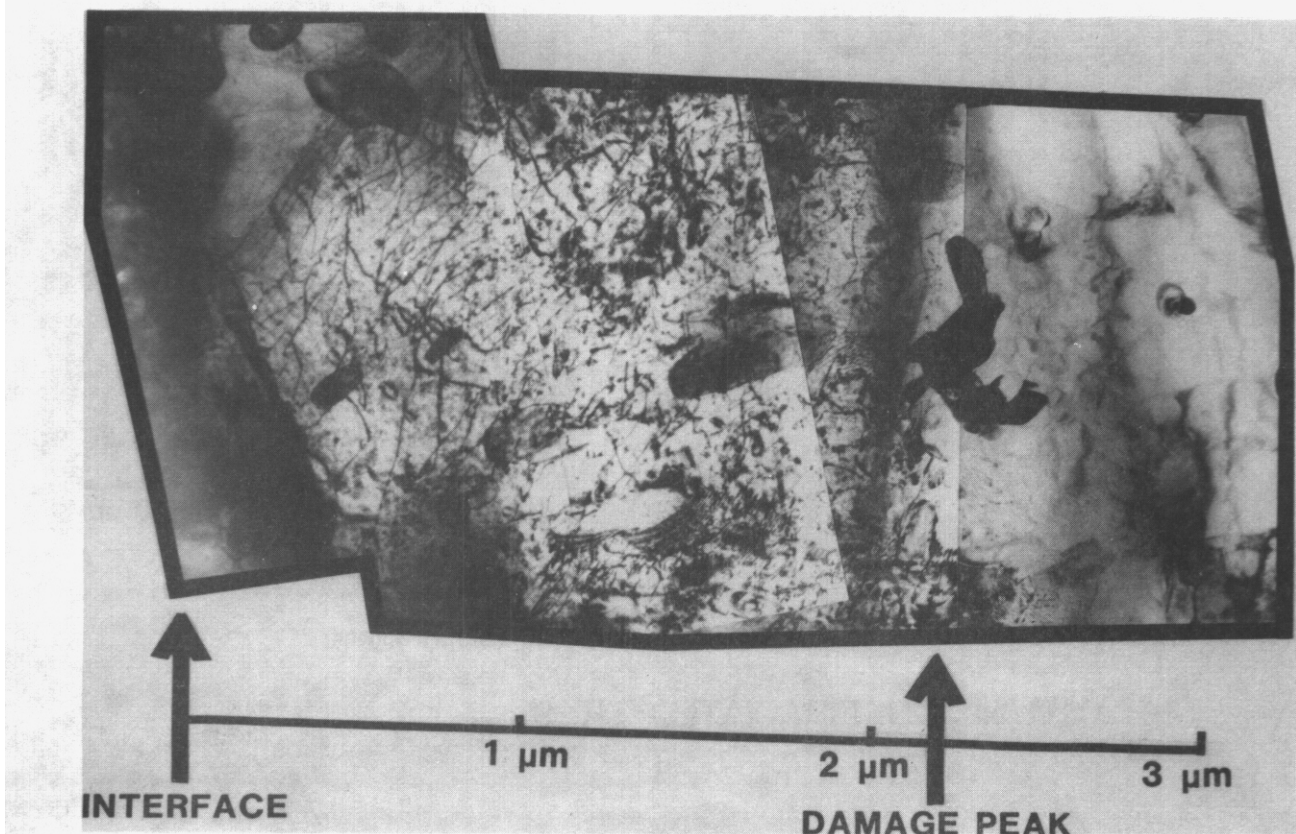


FIGURE 8. TEM microstructures of HT-9 irradiated at 500°C, 8×10^{20} ions/m².

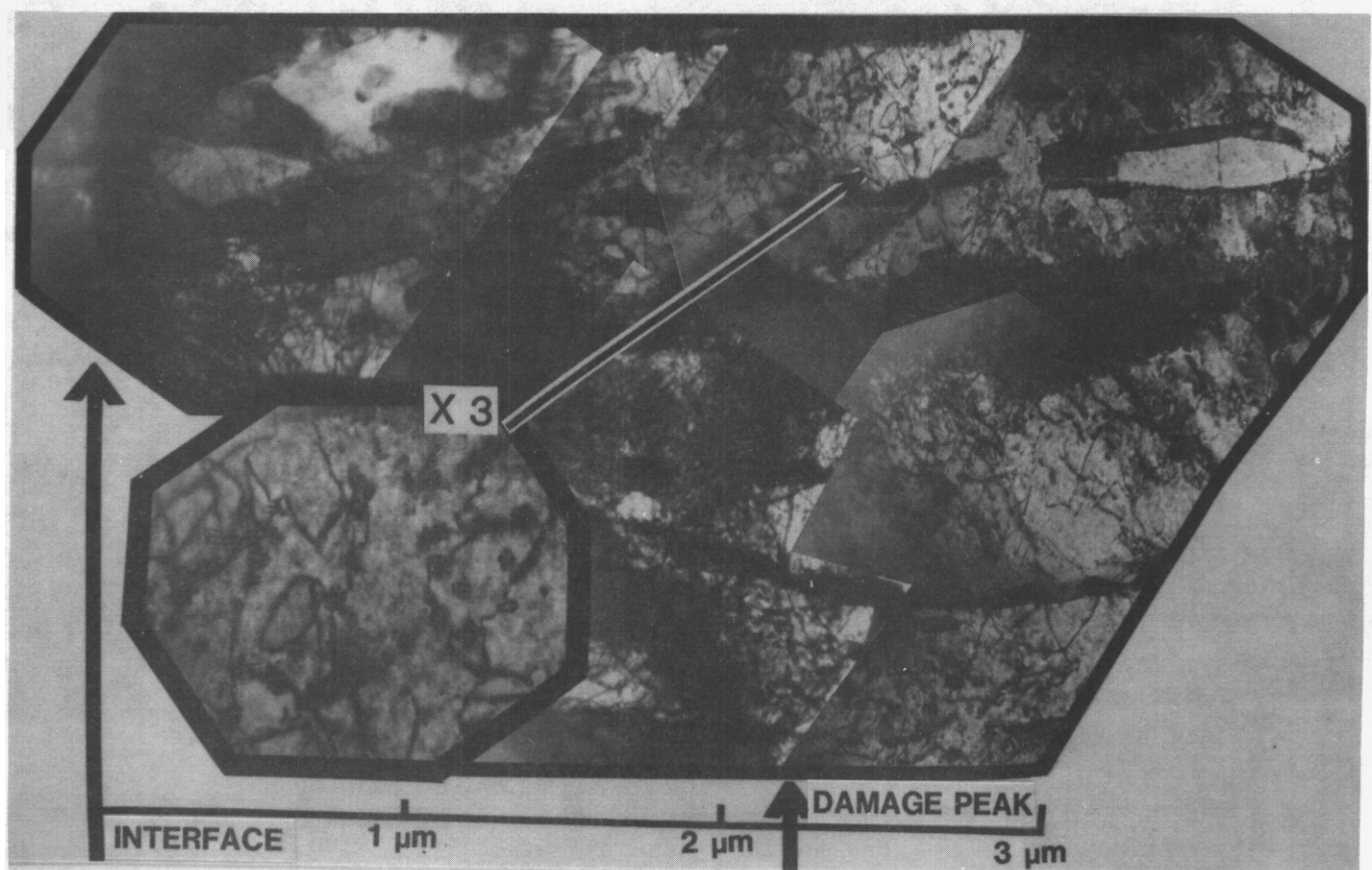


FIGURE 9. TEM microstructures of HT-9 irradiated at 500°C, 13×10^{20} ions/m².

CHI PHASE EVOLUTION IN HT-9
IRRADIATED AT 500°C

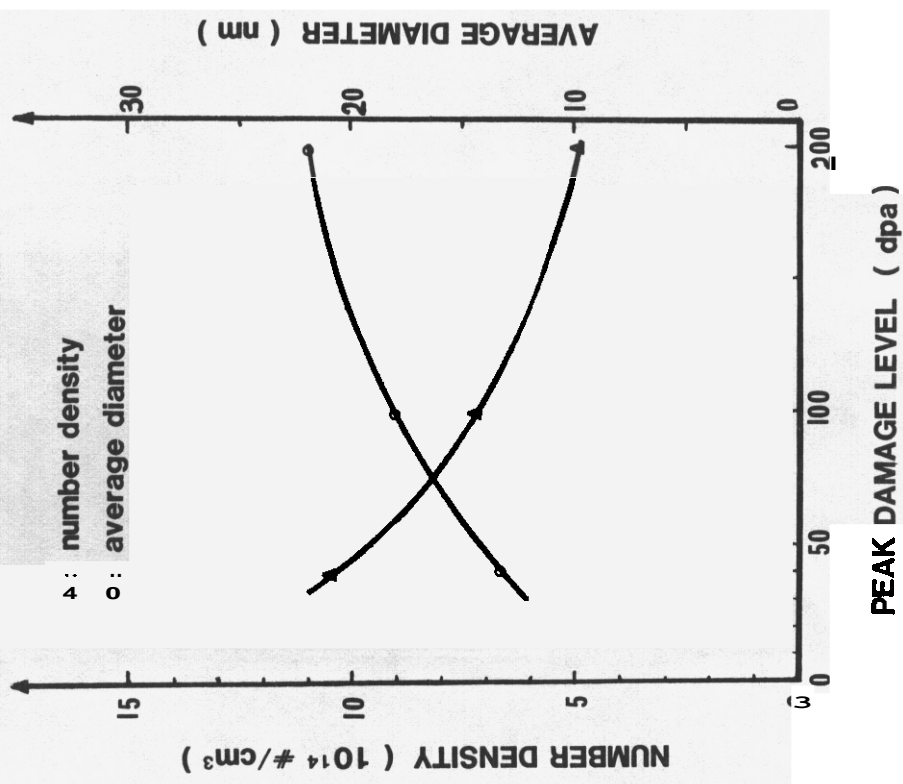


FIGURE 10. The number density vs. chi phase vs. dose level.

the average diameter of

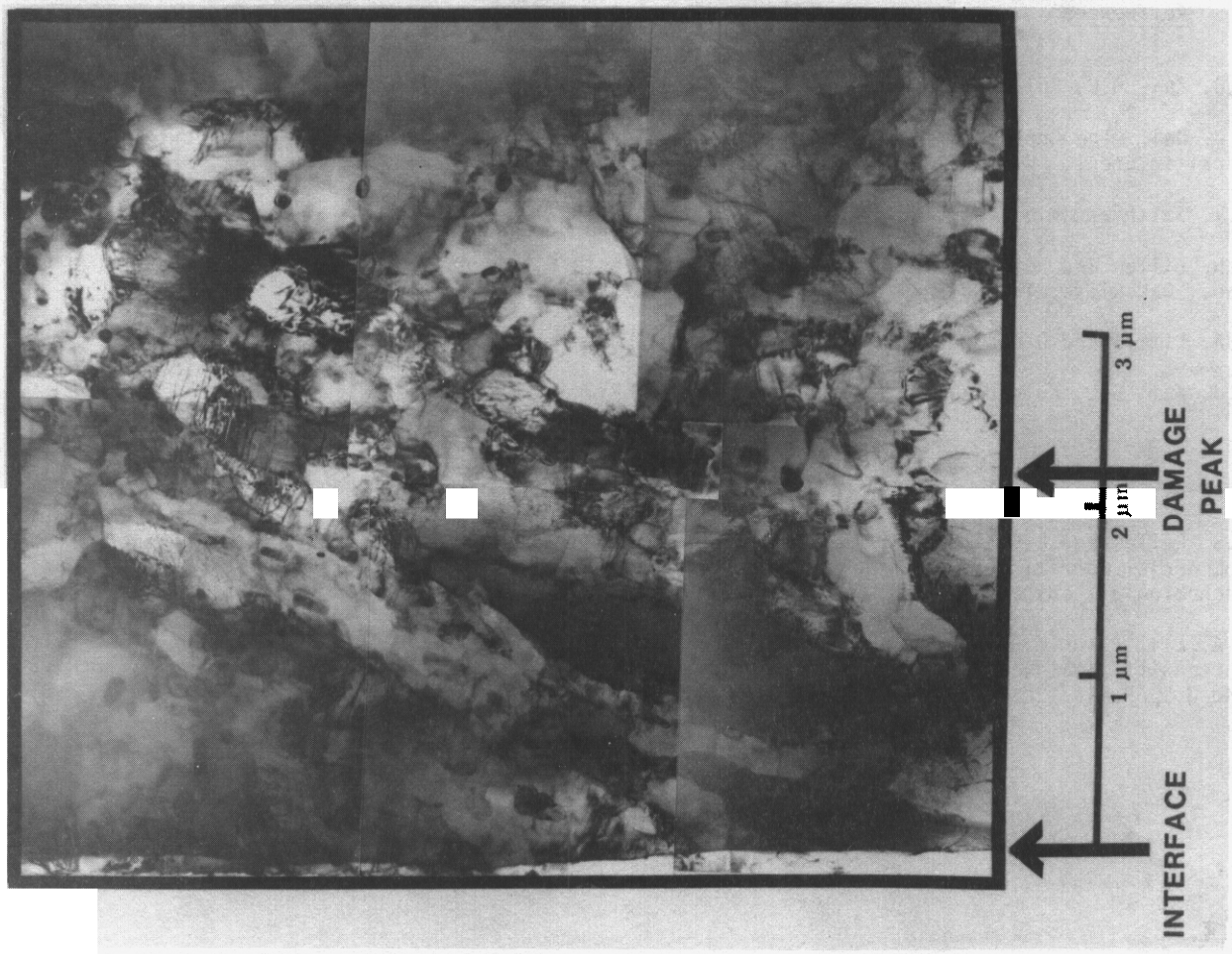


FIGURE 11. TEM microstructures of HT-9 irradiated at 600°C, 3×10^{20} dpm/m^2 .

8.0 References

1. J.J. Kai, G.L. Kulcinski and R.A. Dodd, DAFS DOE/ER-0046/20, pp. 63-67 (Jan. 1985).
2. J.J. Kai, "The Cross-Section Techniques for Preparing TEM Specimens of Heavy Ion Irradiated HT-9 Ferritic Steel," UUFOM-643.
3. H.V. Smith and R.G. Lott, Nucl. Instr. Methods 143 (1977) 125-132.
4. J.H. Billen and H.T. Richards, Proc. of Symp. of Northeastern Accelerator Personnel, Oak Ridge Nat. Lab., Oak Ridge, TN, Oct. 1978, p. 137.
5. E.A. Little and D.A. Sew, Metal Science, March **1980**, pp. 89-94.
6. J.J. Kai, G.L. Kulcinski and R.A. Dodd, DAFS DOE/ER-0046/21, April 1985.

7. E.A. Little, R. Bullough and M.H. Wood, Proc. Royal Sci. London A372 (1980) 565-579.
8. O.S. Gelles and L.E. Thomas, "Effects of Neutron Irradiation on Microstructure in Experimental and Commercial Ferritic Alloys," in the Proc. of Topical Conf. on Ferritic Alloys for Use in Nuclear Energy Technologies, edited by J.W. Davis and D.J. Michel, Snowbird, Utah, 1983.
9. E.A. Little and L.P. Stoter, "Microstructural Stability of Fast Reactor Irradiated **10-12% Cr Ferritic-Martensitic** Stainless Steels," Effects of Radiation on Materials 11th Conf., ASTM-STP-702, H.R. Brager and J.S. Pemini, Eds., ASTM 1982, pp. 207-233.

EFFECTS OF CAVITATION ON DAMAGE CALCULATIONS IN ION-IRRADIATED P7 ALLOY

R.L. Sindelar, S.N. Farrens, and G.L. Kulcinski (University of Wisconsin-Madison)

1.0 Objectives

To investigate the effect of voids on the depth-dependent damage energy in ion-irradiated metals. Corrections to the dose at the swelling peak will be used to obtain the swelling rate of ion-irradiated 316-type stainless steels.

2.0 Summary

Samples of the P7* alloy were ion-irradiated to four fluence levels up to a peak dose level of 100 dpa at 650°C. The depth-dependent void parameters extracted in cross section were used to model the effect of voids on the depth-dependent damage produced during 14 MeV nickel ion irradiation. An increase in the range of damage produced from the original foil surface for the target containing voids was modeled as a first-order correction to the damage profile. A second-order effect, void straggling, was shown to cause a time-dependent decrease in the damage rate at the peak swelling depth. Corrections applied to the dose at the peak swelling depth yield swelling rates approaching 0.7%/dpa.

3.0 Program

Title: Radiation Effects to Reactor Materials
Principal Investigators: GL Kulcinski and R.A. Dodd
Affiliation: University of Wisconsin-Madison

4.0 Relevant DAES Program Task/Subtask

Subtask III.B.2.3 Correlation Methodology

5.0 Accomplishments and Status

5.1 Introduction

For the past several years, neutron-irradiated austenitic stainless steels have been reported to show a 1%/dpa post-transient swelling rate.^{1,2} All austenitic stainless steels seem to exhibit this response regardless of differences in major and minor solute content,^{3,4} irradiation temperature,^{5,6,7} initial degree of cold work⁸ or helium content.⁹ Wolfer and Garner¹⁰ have recently discussed the insensitivity of the swelling rate to these parameters and have predicted a constant swelling rate for a system of large voids and dislocations which have sink strength parity¹¹ and a total sink strength of $5 \times 10^{10} \text{ cm}^{-2}$. This microstructure appears to occur at the 2-10% swelling level in neutron-irradiated 316 SS.² After this density is achieved, the alloy swells at the rate of 1%/dpa. HVEM studies of 316 SS have shown swelling rates of 1%/dpa for a microstructure which had been seeded with voids.¹²

*P7 is essentially a high purity 316 stainless steel prepared at Oak Ridge National Laboratory.

On the other hand, many ion irradiation studies of austenitic stainless steels have shown a swelling rate of only 0.2-0.4%/dpa.¹³⁻¹⁵ Garner¹ has attributed this reduced rate to the action of the injected interstitials on void swelling. This hypothesis is based on work by Johnston¹⁶ who observed anomalous subsurface swelling in 4 MeV nickel-ion-irradiated 304 SS, and Whitley¹⁷ who observed 0.8%/dpa swelling at near-surface depths in 14 MeV nickel-ion-irradiated nickel. Garner concludes that swelling rates under ion irradiation will approach 1%/dpa if data is extracted at depths other than those of the bombarding ion range. We have reported¹⁸ no anomalous subsurface swelling, however, in samples of the P7 alloy irradiated at 650°C. In addition, suppression effects on void swelling in the P7 alloy are not observed at temperatures > 550°C.^{19,20} Yet the results of our swelling rate study (see Figure 1) show only a 0.4%/dpa rate for swelling levels of 35% and doses to 100 dpa.

Mansur and Yoo²¹ have also suggested that a lower swelling rate for heavy ion bombardment studies would occur if the injected ion species caused a large depletion in void growth rates near the peak of point defect production. This effect on void growth is important in systems with a low bias, low sink strength, and high vacancy migration energy. Using a net bias of 0.8 and a vacancy migration energy of 1.1 eV as suggested by Garner and Wolfer,²² along with the total sink strength of $4 \times 10^{10} \text{ cm}^{-2}$ for the irradiated P7 microstructure, it is seen from Figures 9 and 10 in Ref. 21 that there is less than a 5% decrease in the void growth rate due to the action of the injected interstitials. Diffusional spreading of the point defects down the defect generation gradients can also lead to a decrease in the swelling rate.²¹ However, the absorption mean free path, λ , is $1/\sqrt{S}$, where S is the total sink strength. For our sink strength of $4 \times 10^{10} \text{ cm}^{-2}$, it is estimated that the escape of point defects from the damage peak would be negligible (i.e., < 500 Å).

Another possible explanation for the swelling rate discrepancy lies within the dose values ascribed to the swelling profile in ion-irradiated targets. Using transport theory for the distribution of deposited energy, Wolfer and Benchikh-Lehocine²³ have considered the effect of density changes on the damage energy profile. They did not model the discrete nature of void formation but rather they homogenized the swelling at a particular depth into a uniform density decrease at that depth. Effects of a discrete distribution of voids on the deposited energy (damage) has been addressed by Odette et al.²⁴ In the present study, we have applied the model of Odette²⁴ to estimate the accumulated dose at a particular mass depth (e.g., the peak swelling depth) during the 14 MeV nickel ion irradiation of the P7 alloy.

5.2 Experimental

The irradiation parameters of the P7 alloy are given in Table 1. Details of the 14 MeV heavy-ion irradiation and post-irradiation analysis are given in an earlier report.²² Figure 2 shows the damage profile for 14-MeV Ni ions on the void-free P7 target. Figure 3 displays the through-range TEM micrographs of samples irradiated to peak damage levels of 10 and 40 dpa. No void suppression effects are observed in these cross-sectioned foils. The depth-dependent void parameters of the irradiated P7 samples are contained in the earlier report.¹⁸

5.3 Model of Damage Profile in a Target with Voids

Following the notation of Odette et al.²⁴ we let $\lambda(y)$ be the distance within voids through which the bombarding particle has passed upon reaching depth y . That is, a charged particle that penetrates a depth x in a solid target would penetrate a distance y in void-containing material where

$$y = x + \lambda(y) \quad (1)$$

The average value of $\lambda(y)$, $\langle \lambda(y) \rangle$, can be calculated from the volume fraction of voids, $\Phi(y)$, by

$$\langle \lambda(y) \rangle = \int_0^y \Phi(y') dy' = \int_0^y \frac{S}{1+S} dy' \quad (2)$$

where y' is the integration variable and S is the local swelling, defined by the ratio of void volume to original volume.

P7 SWELLING -14 MeV NI ION IRRADIATION

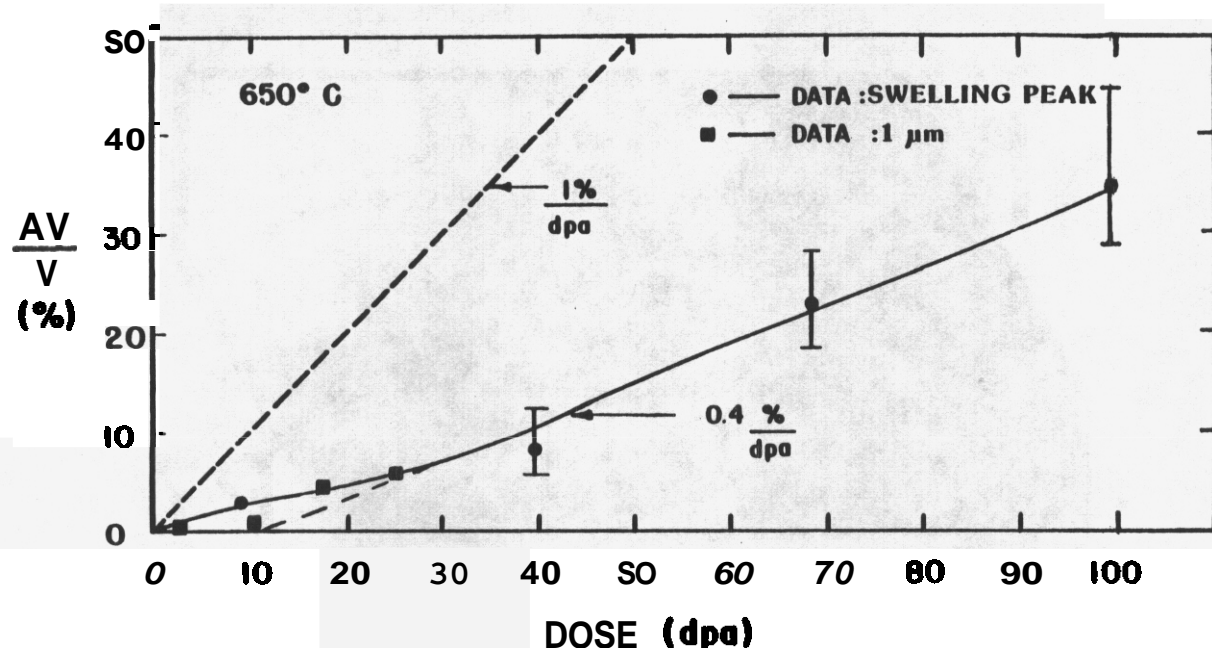


FIGURE 1. Swelling rate in 14 MeV ion-irradiated P7 alloy.

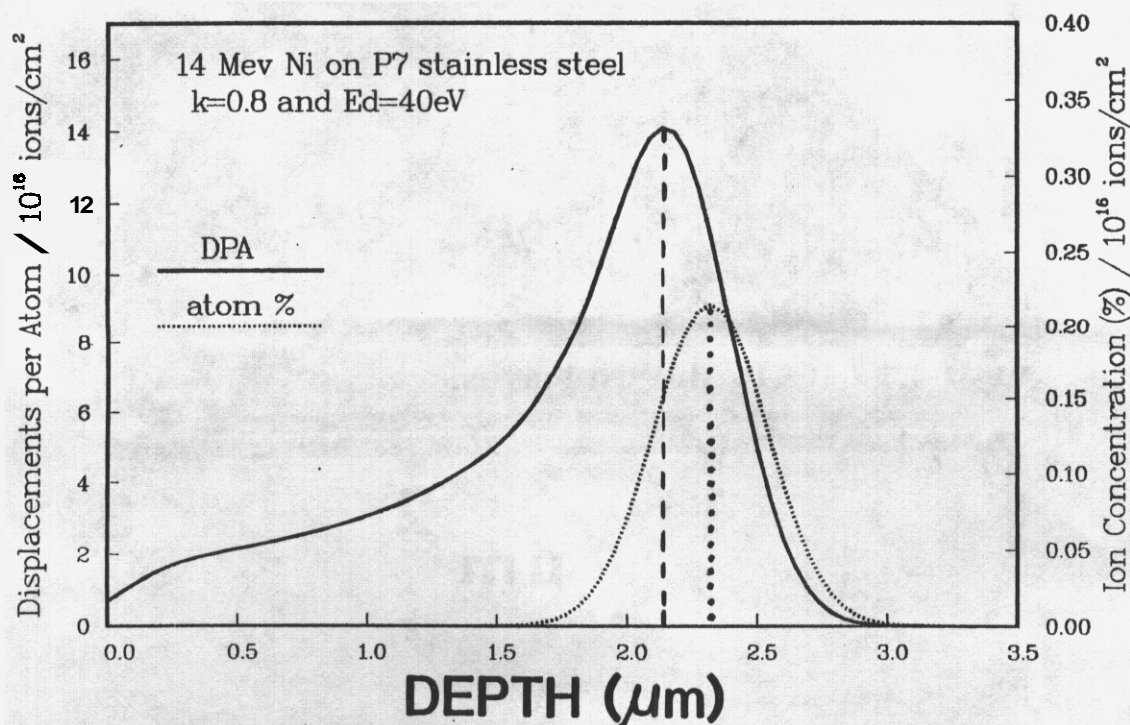


FIGURE 2. Damage (dpa) vs. distance from the irradiated surface calculated using the Brice code. The damage efficiency (K) used is 0.8. $E_d = 40$ eV.

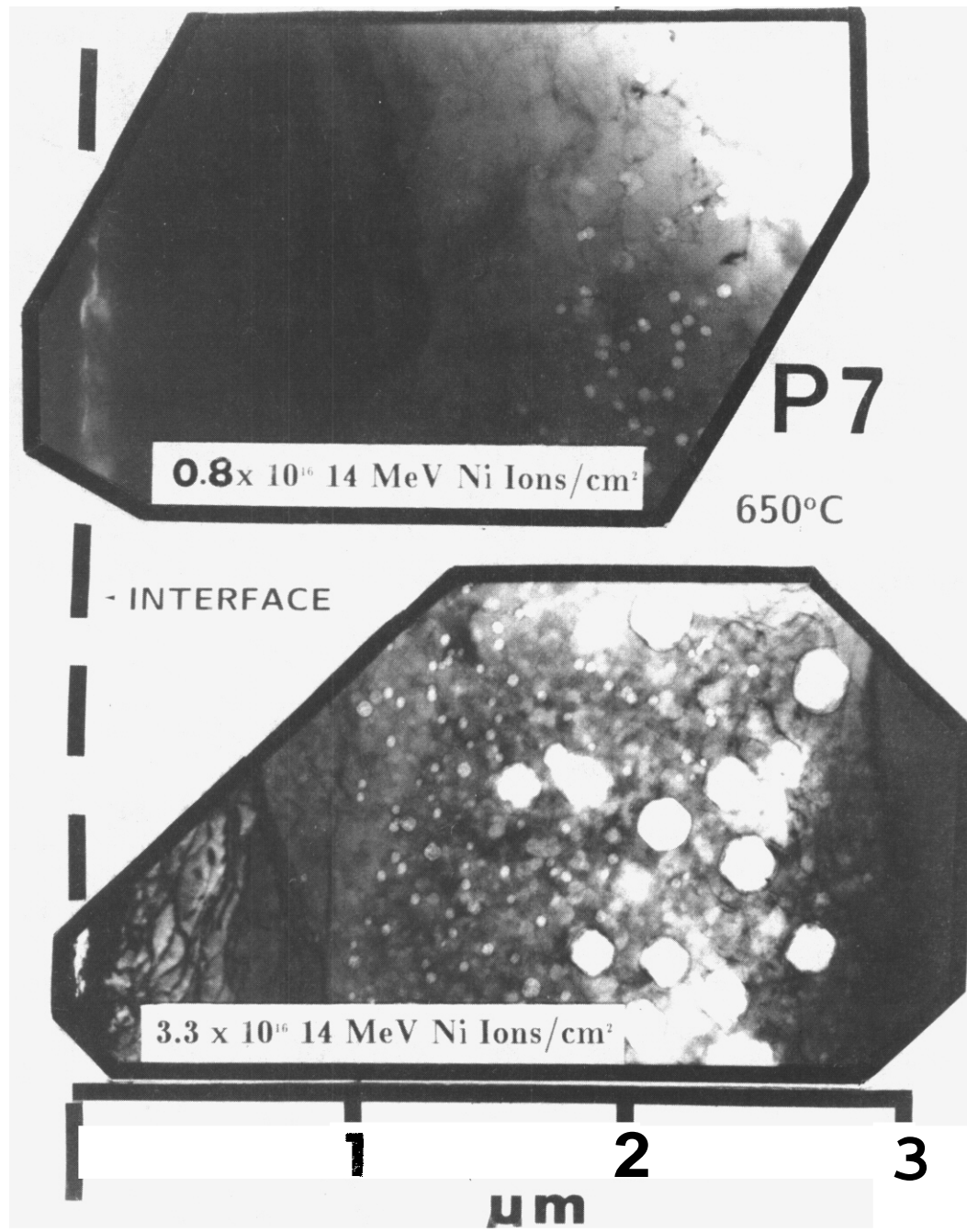


FIGURE 3. 14-MeV Ni ion-irradiated P7 to peak doses of 10 and 40 dpa for 0.8 and 3.3×10^{16} ions/cm⁻²

TABLE 1

PARAMETERS FOR A 14-MeV Ni-ION IRRADIATION OF P7
DISPLACEMENT EFFICIENCY $K = 0.8$, $E_d = 40$ eV, $T_{irr} = 650^\circ\text{C}$

dpa at 1 μm	Peak dpa	Fluence (ions/cm 2)
2.3	20	0.8×10^{16}
10	40	3.3×10^{16}
17*	68*	$5.6 \times 10^{16}\star$
25	100	8.3×10^{16}

*Damage rate at 1 μm from surface is 1.6×10^{-3} dpa/s, at the peak it is 6.4×10^{-3} dpa/s; the other samples were irradiated at 0.8×10^{-3} dpa/s at 1 μm and 3.2×10^{-3} dpa/s at the peak damage region.

Heavy ion irradiation damage is created by a unidirectional beam of projectiles and thus is subject to statistical fluctuations in the energy of the particles at a certain depth based on the number of atomic collisions (prior history) the particles have undergone. This effect is well-known as Bragg straggling²⁵ and is the intrinsic straggling associated with energy deposited in a solid target. In a void-containing target, the distance traveled through voids by particles reaching depth y will vary as a result of the Statistical fluctuations in the number and sizes of voids a particle encounters. This effect is termed²⁴ "void-straggling" and creates an additional spread in the energy distribution of the particles at depth y which is superimposed on the spread due to intrinsic straggling. The average number of interactions, $\langle n_y \rangle$, between the bombarding ions and voids can be given by

$$\langle n_y \rangle = \langle \lambda(y) \rangle / D \quad (3)$$

where D is a characteristic void length, equivalent to length of the average track of the void. Noting that the average chord length of a sphere of radius R is given by $413 R$, we will use

$$D = 213 D_{ave} \quad (4)$$

where D_{ave} is the average void diameter.

Next we will approximate the distribution of the number of voids that the particle hits as a Poisson distribution.²⁶ Thus $\langle n_y \rangle$ is equal to σ_n^2 , the variance of the number of voids encountered. Now the standard deviation in the total length through voids traversed upon reaching depth y can be given by σ_λ ,

$$D\sqrt{\langle n_y \rangle} = \sqrt{D\langle \lambda(y) \rangle} . \quad (5)$$

During the irradiation of a high-swelling material, both $\langle \lambda(y) \rangle$ and D will increase with depth. Thus the void-straggling phenomenon will create an increasing energy spread at a given mass depth as the irradiation proceeds.

The energy deposition at y is now written as:²⁴

$$S_D(y) = [1 - \Phi(y)] \int_0^\infty f(R) \int_{\lambda_{min}}^y P(\lambda) S_A(R-y+\lambda) d\lambda dR \quad (6)$$

where $f(R)$ is the probability distribution function which describes intrinsic straggling^{27,28} and $S_A(R-y+\lambda)$ is the deposited (damage) energy for a particle with energy $E(R-y+\lambda)$ where $R-y+\lambda$ is the residual solid range of the particle. $P(\lambda)$ is the probability distribution function which describes the void-induced straggling, with λ_{min} given by

$$A_{min} = \begin{cases} 0, & y < R \\ y - R, & y > R \end{cases}$$

Equation (6) neglects the influence of secondary atom energy transport and does not correct for secondary energy partition. We have used a first-order estimate for $P(\lambda)$ as a normalized Gaussian distribution with parameters $\langle\lambda\rangle$ given by Eq. (2) and σ_λ given by Eq. (51).

5.4 Dpa Profile in P7 with Voids

The factor $1-\Phi(y)$ in Eq. (6) does not change the dpa value at depth y since the dpa unit is defined for solid material. Also, using the Brice code (see Figure 2) to calculate the dpa profile with intrinsic straggling for void-free material, we can reduce Eq. (6) to simply

$$dpa(y) = \int_{\lambda_{min}}^y P(\lambda) dpa(\lambda-y) d\lambda \quad (7)$$

to calculate the instantaneous dpa rate at y in the P7 target with voids.

5.5 Results

We have applied a simple first-order estimate to the void-straggling phenomenon by using a single set of parameters, $\langle\lambda\rangle$ and σ_λ for $P(\lambda)$. Figure 4 displays the depth-dependent instantaneous dpa rate in the P7 target for cases:

- | | |
|---|---|
| 1. $\langle\lambda\rangle = 0.3 \text{ } \mu\text{m}$, $\sigma_\lambda = 0.2 \text{ } \mu\text{m}$ | 2. $\langle\lambda\rangle = 0.2 \text{ } \mu\text{m}$, $\sigma_\lambda = 0.14 \text{ } \mu\text{m}$ |
| 3. $\langle\lambda\rangle = 0.07 \text{ } \mu\text{m}$, $\sigma_\lambda = 0.08 \text{ } \mu\text{m}$ | 4. $\langle\lambda\rangle = 0.02 \text{ } \mu\text{m}$, $\sigma_\lambda = 0.03 \text{ } \mu\text{m}$. |

These parameters, valid at the peak swelling depth, were computed from the void parameters of the P7 samples given in our earlier report.¹⁷ Note the finite decrease in dpa rate with increasing $\langle\lambda\rangle$ and σ_λ . This decrease, termed second-order void straggling effects, will cause a decrease in the dpa rate to occur with time (dose) at a given mass depth for the high-swelling P7 alloy.

5.6 Discussion

Consideration of these effects of cavitation on the dpa rate of the P7 samples irradiated at 650°C has led to the correction of the swelling versus dpa curve shown in Figure 1. Figure 5 displays the curve which is modified to account for the real decrease in dpa at a given mass depth (e.g., swelling peak). The accumulated dose levels are determined by integration of the damage rates given in Figure 4. It is seen from Figure 5 that the second-order effects become important at swelling levels of 20%. The large ~ 200 nm voids are responsible for the large value of the void-straggling parameter at these swelling levels. The corrected swelling rate of the P7 alloy approaches 0.7%/dpa after a transient dose of 50 dpa and swelling levels ~ 10%.

Although several possible mechanisms¹⁸ may account for the swelling rate discrepancy of heavy ion data with neutron data, the void size and density distribution 14 MeV Ni ion-irradiated P7 necessitate the correction of the accumulated dose at the peak swelling depth. Simple first-order corrections applied to the accumulated dose have shown that the void-straggling phenomenon acts to reduce the dpa value at a given mass depth. More accurate calculations are needed however to give a better estimate of the accumulated dose at a given mass depth.

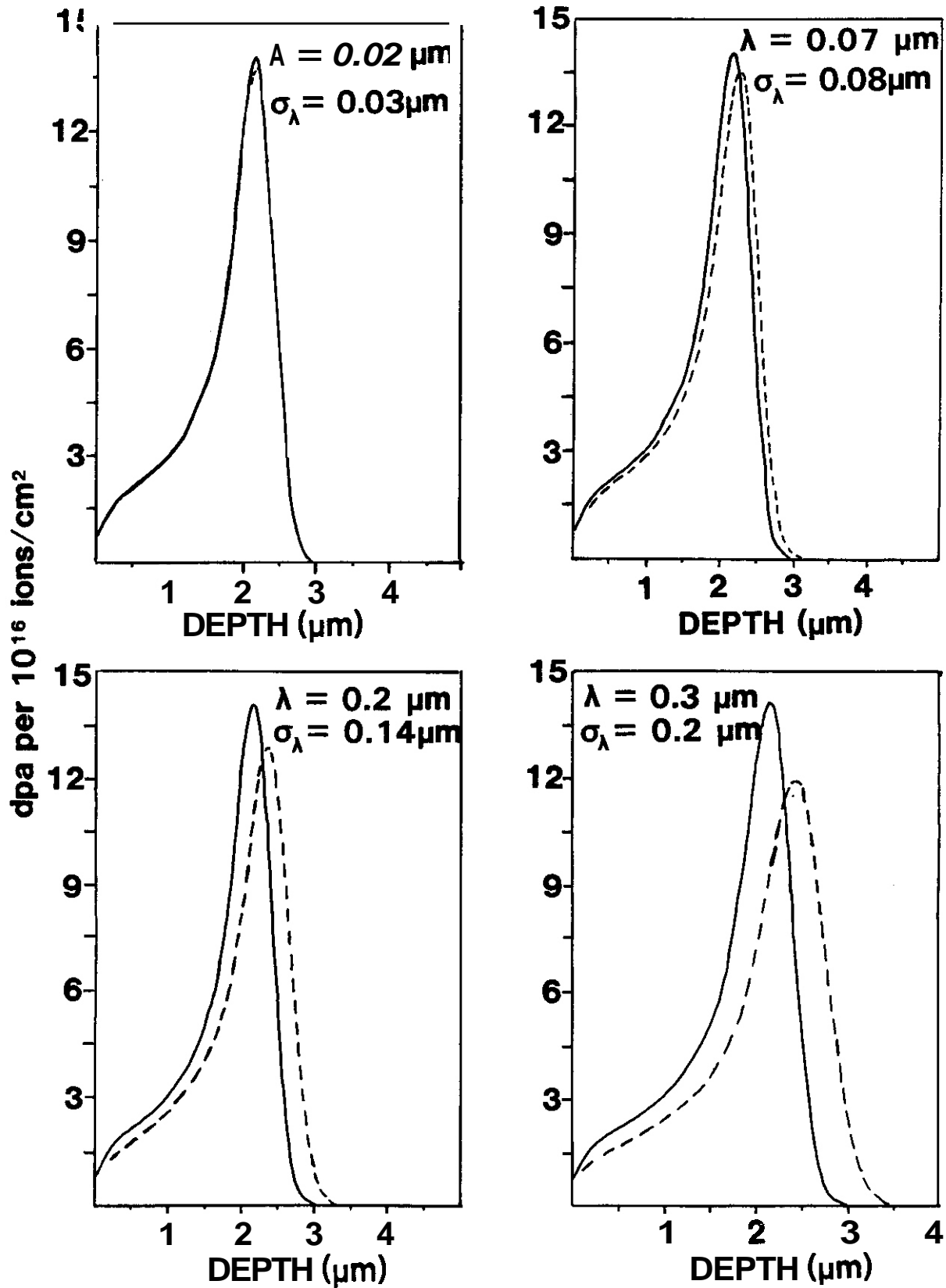


FIGURE 4. Dpa rate in P7 with voids. Damage profile calculated from Eq. (7) with a constant $P(\lambda)$.

P7 SWELLING -14 MeV Ni ION IRRADIATION

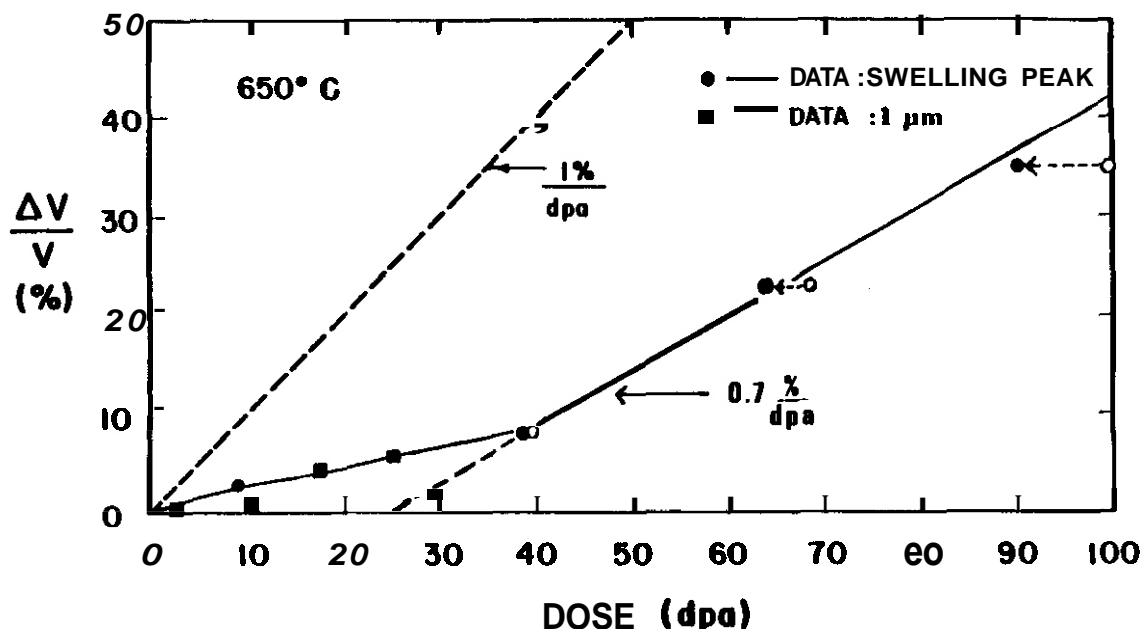


FIGURE 5. Swelling rate of P7 with dose levels corrected to account for void-straggling effects. Note that the dose level correction increases with swelling.

5.7 Conclusions

Simple consideration of cavitation on the dpa profile to account for void-straggling effects has led to the correction of the swelling rate determined for 14 MeV Ni ion-irradiated P7. Post-transient rates were 0.7%/dpa, which approach those observed during fast neutron irradiation.

6.0 References

1. F.A. Garner, J. Nucl. Mat. 117 (1983) 177.
2. F.A. Garner, J. Nucl. Mat. 122&123 (1984) 459.
3. W.J.S. Yang and F.A. Garner Effects of Radiation on Materials: Eleventh Conference, ASTM STP 782, H.R. Brager and J.S. Perrin, Eds., (1982) 186.
4. J.F. Bates and W.G. Johnston, "Effects of Alloy Composition on Void Swelling" in Radiation Effects in Breeder Reactor Structural Materials, M.L. Bleiberg and J.W. Bennett, Eds. TMS-AIME (1977) 543.
5. J.L. Seran and J.M. Dupouy, Ref. 3, p. 5
6. J.L. Seran and J.M. Dupouy, Ref. 4, p. 25.
7. F.A. Garner, in Proc. of AIME Symp. on Phase Stability During Irradiation, Pittsburgh, 1980, 165.
8. F.A. Garner, DAFS Quarterly Progress Report DOE/ER-0046/12 (Feb. 1983) 178.
9. H.R. Brager and F.A. Garner, J. Nucl. Mat. 117 (1983) 159.
10. F.A. Garner and W.G. Wolfer, J. Nucl. Mat. 122&123 (1984) 201.
11. W.G. Wolfer, ibid., 367.

12. M.J. Makin et al.. J. Nucl. Mat. 95 (1980) 155-170.
13. W.G. Johnston et al., "The Effect of Metallurgical Variables on Void Swelling", in Radiation Damage in Metals, ASM (1976) 177.
14. N.H. Packan and K. Farrell, J. Nucl. Mat. 85&86 (1979) 677.
15. K. Farrell and N.H. Packan, ibid., 683.
16. W.G. Johnston, W.G. Morris and A.M. Turkalo, in Ref. 4, p. 421.
17. J.B. Whitley, Ph.D. Thesis, University of Wisconsin-Madison, 1974.
18. R.L. Sinalar, S.J. Zinkle and G.L. Kulcinski, DAFS Quarterly Progress Report DOE/ER-0046/20 (Feb. 1985).
19. B. Badger, Jr., et al., ASTM STP 870.
20. R.L. Sindelar. Ph.D. Thesis, University of Wisconsin-Madison, 1985.
21. L.K. Mansur and M.H. Yoo, J. Nucl. Mat. 85&86 (1979) 523.
22. F.A. Garner and W.G. Wolfer, J. Nucl. Mat. 122&123 (1984) 201.
23. W.G. Wolfer and M.E. Denchikh-Lehocine, DAFS Quarterly Progress Report DOE/ER-0046/20 (Feb. 1985).
24. G.R. Odette, D.M. Schwartz and A.J. Ardell, Rad. Effects 22 (1974) 217-223.
25. R. Evans, The Atomic Nucleus (McGraw-Hill, New York, 1955) p. 666.
26. Ibid.. p. 660.
27. G.L. Kulcinski, J.J. Laidler and D.C. Doran, Rad. Effects 7 (1971) 195.
28. I. Manning and G.P. Mueller, Computer Physics Comm 7 (1974) 05-94.

EXTERNAL DISTRIBUTION

UC-20 (108), 20c (60)

DOE-HQ/Office of Fusion Energy
ER-62
Washington, DC 20545

SE Parket

DOE-HQ/Office of International Security Affairs
DP-33, Mail Stop 4C-024
Washington, DC 20585

DW Dorn

Argonne National Laboratory (3)
9700 South Cass Avenue
Argonne, IL 60439

LR Greenwood, CMT-205
A. Taylor, MST-212
BA Loomis, MST-212

Argonne National Laboratory
EBR-II Division
Reactor Materials Section
P.O. Box 2528
Idaho Falls, ID 83403-2528

DL Porter

Battelle Pacific Northwest Laboratory (2)
P.O. Box 999
Richland, WA 99352

JL Brimhall 306W/210
TD Chikalla PSL/1277

Carnegie-Mellon University
Metallurgical Engineering
3325 Science Hall
Pittsburgh, PA 15213

WM Garrison Jr

Centre d'Etudes de Chimie Metallurgique
15, Rue Georges-Urbain
Vitry-sur-Seine
94400 Vitry, France

G. Martin

Columbia University
School of Engineering & Applied Science
New York, NY 10027

RA Gross

Commission of the European Communities
Rue de la Loi 200
B-1049 Bruxelles, Belgium

J. Darvas

Commission of the European Communities (2)
Joint Research Center
I-21020 Ispra, Varese, Italia

R. Dierckx, Physics Division
P. Schiller, Materials Science Division

Department of the Navy
Naval Research Laboratory (2)
Washington, DC 20375

JA Sprague, Code 6395
LE Steele, Code 6390

Energieonderzoek Centrum Nederland (7)
Netnlands Energy Research Foundation
Westerduinweg 3, Postbus 1
NL-1755 ZG Petten (NH), The Netherlands

B. vanderSchaaf
W. vanWitzenburg, Materials Dept

GA Technologies Inc (3)
P.O. Box 85608
San Diego, CA 92138

JR Gilleland
GR Hopkins
T. Lechtenberg

General Dynamics/Convair
P.O. Box 85377
San Diego, CA 92138

H. Gurol, MZ 92-1072

General Electric
Advanced Nuclear Technology Operation (2)
310 DeGuign Drive
Sunnyvale, CA 94088

ANTO Library, M/C F-02
S. Vaidyanathan, M/C 5-53

Hahn-Meitner Institut fur Kernforschung Berlin GmbH
Arbeitsgruppe C2
Glienickerstrasse 100
D-1000 Berlin 39, Federal Republic of Germany

H. Wollenberger

Hokkaido University (2)
Facility of Engineering
Kita-hu, Sapporo, 060 Japan

Michio Kiritani, Precision Engineering
Taro Takeyama, Metals Research Institute

Institut fur Festkorperforschung der
Kernforschungsanlage Juelich GmbH
Postfach 1913
D-5170 Juelich 1, Federal Republic of Germany

P. Jung

EXTERNAL DISTRIBUTION (Cont'd)

Japan Atomic Energy Research Institute (2)
Physical Metallurgy Laboratory
Tokai Research Establishment
Tokai-mura, Naka-gun, Ibaraki-ken, 319-11 Japan

Tadao Iwata, Physics
Kensuke Shiraishi, Fuels Materials Research

Kernforschungszentrum Karlsruhe GmbH
Institut fur Material und Festkorperforschung II
Postfach 3640
D-7500 Karlsruhe 1, Federal Republic of Germany

K. Ehrlich

Kyushu University
Research Institute for Applied Mechanics
6 Kasuga-Koen, Kasuga-shi
Fukuoka, 816 Japan

Kazunori Kitajima

Lawrence Livermore National Laboratory (2)
P.O. Box 808
Livermore, CA 94550

MW Guinan, L-396
DW Heikkinen, L-397

Lawrence Livermore National Laboratory
P.O. Box 5511
Livermore, CA 94550

EC Dalder, L-643

Los Alamos National Laboratory
P.O. Box 1663
Los Alamos, NM 87544

DJ Dudziak, S-41F611

Massachusetts Institute of Technology (2)
77 Massachusetts Avenue
Cambridge, MA 02139

I-Wei Chen, 13-5118
NJ Grant, 8-407

Massachusetts Institute of Technology
Nuclear Reactor Laboratory
138 Albany St
Cambridge, MA 02139

OK Harling, NW12-204

Max-Planck-Institut fur Plasma Physik (2)
The NET Team, IPP/NET
D-8046 Garching bei München,
Federal Republic of Germany

DR Harries
R. Toschi

McDonnell-Douglas Astronautics Co
P.D. Box 516
St. Louis, MO 63166

JW Davis

Nagoya University
Institute of Plasma Physics
Euro-chyo, Chikusa-ku,
Nagoya, 464 Japan

Taijiro Uchida

National Research Institute for Metals
Tsukuba Laboratories
1-2-1 Sengen, Sakura-mura,
Nihari-gun, Ibaraki, 305 Japan

H. Shiraishi

North Carolina State University
Box 7907
Materials Engineering Department
Raleigh, NC 27695-7907

JR Beeler Jr

Oak Ridge National Laboratory (7)
P.O. BOX X
Oak Ridge, TN 37831

ML Grossbeck PJ Maziasz
MCG Hall NH Packan
LK Mansur RE Stoller
SJ Zinkle

Oak Ridge National Laboratory (2)
P.O. BOX Y
Oak Ridge, TN 37831

LA Berry
FW Wiffen, FEDC Bldg

Osaka University
2-1 Yamada-oka, Suita,
Osaka, 565 Japan

Kenji Sumita, Nuclear Engineering

Osaka University
8-1 Mihogaoka
Ibaraki, Osaka, 567 Japan

Toichi Okada, Institute of
Scientific & Industrial Research

Pacific Sierra Research Corp
1104B Camino Del Mar
Del Mar, CA 92014

RD Stevenson

EXTERNAL DISTRIBUTION (Cont'd)

Princeton University (2)
Plasma Physics Laboratory
Forrestal Campus
P.O. Box 451
Princeton, NJ 08544

JPF Conrads
Long-poe Ku

Rism National Laboratory
Postfach 49
DK-4000 Roskilde, Denmark

BN Singh

Rockwell International Corp
Rocketdyne Division
6633 Canoga Avenue
Canoga Park, CA 91304

DW Kneff, NA02

Sandia National Laboratories
Livermore, CA 94550

WG Wolfer

Science University of Tokyo
Faculty of Engineering
Kagurakawa, Shinjuku-ku,
Tokyo, 162 Japan

RR Hasiguti

Studiecentrum voor Kernenergie
Centre d'Etude de l'Energie Nucleaire
Boeretang 200
B-2400 Mol, Belgium

J. Nihoul

Swiss Federal Institute
for Reactor Research (2)
CH-5303 Würenlingen, Switzerland

WV Green
M. Victoria

Tohoku University (2)
Research Institute for Iron,
Steel and Other Metals
2-1-1 Katahira, Sendai, 980 Japan

Katunori Abe
Hideki Matsui

Tokyo Institute of Technology
Research Laboratory for Nuclear Reactors
12-1, 2-chome, O-Okayama
Meguro-ku, Tokyo, 152 Japan

Kazutaka Kawamura

United Kingdom Atomic Energy Authority
Atomic Energy Research Establishment (2)
Oxfordshire OX11 ORA, UK

R. Bullough, Theoretical Physics

United Kingdom Atomic Energy Authority
Culham Laboratory
Applied Physics & Technology Division
Abingdon, Oxfordshire OX14 3QB, UK

GJ Butterworth

University of California (2)
School of Engineering and Applied Science
Boelter Hall
Los Angeles, CA 90024

RW Conn, KL-98
NM Ghoniem, KH-01

University of Michigan
Nuclear Engineering
Ann Arbor, MI 48109

T. Kamash

University of Missouri
Dept of Nuclear Engineering
Rolla, MO 65401

A. Kumar

University of Tokyo (3)
3-1, Hongo 7-chome,
Bunkyo-ku, Tokyo, 113 Japan

Naohira Igata, Met & Materials Science
Shiori Ishino, Nuclear Engineering
Shuichi Iwata, Nuclear Engineering

University of Virginia
Dept of Materials Science
Thornton Hall
Charlottesville, VA 22901

WA Jesser

Westinghouse
Advanced Energy Systems Division
Fuels Materials Technology
P.O. Box 10864
Pittsburgh, PA 15236

A. Roltax, Manager

Westinghouse
Research and Development Center
1310 Beulah Road
Pittsburgh, PA 15235

JA Spitrnagel

INTERNAL DISTRIBUTION

DOE-RL/AMF
Site & Laboratory Management Division (SMD)
Laboratory Management & Technology
Services Branch
FED/210-B

KR Absher, Chief

HEDL (28)

HR Brager	W/A-58	C. Martinez	W/A-58
LL Carter	W/B-47	VN McElroy	W/C-39
DG Doran (5)	W/A-57	EK Opperman	W/A-58
MJ Korenko	W/C-27	RW Powell	W/A-58
FA Garner	W/A-58	RJ Puigh	W/A-58
DS Gelles	W/A-58	FA Schmittroth	W/A-58
R. Gold	W/C-39	WF Sheely	W/C-20
HL Heinisch	W/A-58	RL Simons	WIA-65
DL Johnson	W/B-41	JL Straalsund	W/A-61
GD Johnson	W/A-65	HH Yoshikawa	W/C-44
NE Kenny	W/C-115	Central Files	W/C-110
FM Mann	W/A-58	Documentation Services	W/C-123